Chemistry Research Journal, 2024, 9(3):143-170

Available online www.chemrj.org

Research Article

ISSN: 2455-8990
CODEN(USA): CRJHA5

Synthesis, Physico - Chemical, Thermal, Biological and Molecular Docking Studies of Some Sulfasalazine Metal Complexes. Zn (II), Cd (II), Hg (II), Cu-Ni, and Cu-Zn

Riham S. Ibrahim, Alaa E. Ali, Sherif A. Kolkaila* and Gehan S. Elasala

Chemistry Department, Faculty of Science, Damanhour University, Damanhour Egypt.
*Email: sherifkolkaela@yahoo.com

Abstract Three simple sulfasalazine metal complexes of Zn (II), Cd (II) and Hg (II) and two mixed sulfasalazine metal complexes of (Cu(II), Ni(II)) and(Cu(II), Zn(II)) were synthesized and characterized by elemental analysis, IR, electronic spectra, magnetic susceptibility, ESR spectra , mass spectra and X-ray diffraction (XRD) of complexes to know their geometries and mode of bonding, with stoichiometries, 1 :1 (M : L) for simple metal complexes and (1:2:2) (M1: M2: L) for mixed metal complexes. All metal ions complexes were proposed to be with octahedral, distorted octahedral, square planar and tetrahedral geometries. The TGA and DTA curves were employed to derive the kinetic thermodynamic parameters under the N_2 atmosphere. The thermal decomposition of the complexes ended with the formation of metal oxide as a final product. Sulfasalazine complexes showed higher biological activity than sulfasalazine itself for some strains. Molecular docking simulation outcomes a strong binding of sulfasalazine and complexes to the 6XXO (prostate cancer protein).

Keywords Sulfasalazine, Synthesis, Simple complexes, Mixed complexes, Spectral, Mass spectra, XRD, Thermal analysis, biological activity, Molecular docking

1. Introduction

SSZ is a disease-modifying anti-rheumatic medication (DMARD) that is prescribed to rheumatoid arthritis sufferers in several different nations. In the 1950s, sulfasalazine was first used to treat inflammatory bowel disease. At the time, it was also thought to be effective in treating rheumatoid arthritis (RA), since bacterial infections were thought to be the cause of this type of arthritis. It was first used more widely in RA in the late 1970s. It was then used as an anti-inflammatory drug in the long-term, chronic therapy of inflammatory bowel disease (IBD). Sulfasalazine was used in the treatment of IBD as well as other conditions like psoriatic arthritis, juvenile idiopathic arthritis, and Crohn's disease. [1-3].

Sulfasalazine (SSZ), Figure (1), (E)-2-hydroxy-5-[[4-(N-pyridin-2-yl) sulfamoyl) Phenyl] diazenyl] benzoic acid. Sulfasalazine (salazosulfapyridine) is marketed under trade name (Azulfidine, Salazopyrin) [4], SSZ has molecular formula (C18H14N4O5S) and molar mass of 398.39 g/mol. SSZ belongs to class of drugs referred as (sulfa drugs), sulfasalazine is a prodrug which is structurally consists of a derivative of the anti-inflammatory salicylic acid, 5-amino-salicylic acid (mesalamine or mesalazine) and the antimicrobial sulfapyridine, these two moieties are joined together by an azo bond [5-7].

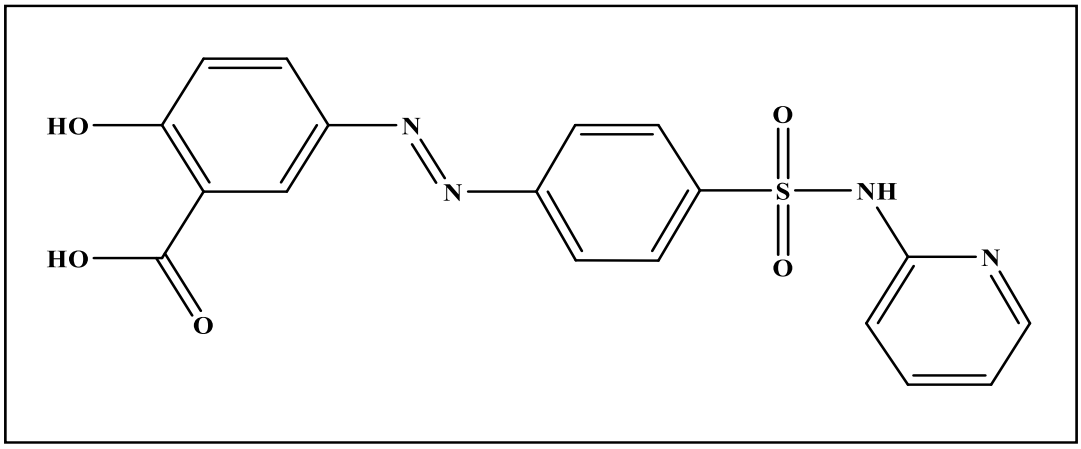

Figure 1: Chemical structure of sulfasalazine

Sulfasalazine (SSZ) is a tasteless, odorless substance that can be seen as tiny, brownish-yellow crystals or as light brownish yellow to bright yellow fine powder [8]. Melting point (measure the temperature at which a solid melt) is a temperature at which solid and liquid coexist at equilibrium, sulfasalazine decomposes before reaching its melting point so decomposition temperature (Td) shall be provided instead, Td of SSZ is (220 ^{o}C). SSZ Practically is insoluble in water, diethyl ether, chloroform, and benzene, very slightly soluble in ethanol and methanol, soluble in aqueous solution of alkali hydroxides, and organic solvent like dimethyl sulfoxide (DMSO) and dimethyl formamide (DMF), the solubility of SSZ in these solvents is approximately 100,30 mg/ml, respectively. SSZ is stable under recommended storage conditions (store SSZ in a closed container at room temperature (25 ^{o}C), away from heat, moisture, and direct light) and when heated to decomposition it emits very toxic fumes of sulfur oxides and nitrogen oxides [9-11].

In recent times, metal complexes have attracted noteworthy interest in several crucial domains, especially when they incorporate the interaction between a metal ion and a pharmacological constituent, resulting in the production of metal complexes. These compounds were shown to have better properties, which made them more significant in several sectors, such as antibacterial, antioxidant, anticancer, and other application-related issues [12, 13].

Certain transition metals can form complexes with SSZ to increase its bioactivity and create brand-new, extremely effective, low-toxicity drugs. SSZ is one of the few sulfanilamides in which the free amino group in the benzene ring is modified and it is synthesized by an azo-coupling reaction of a diazo salt, which is synthesized by reacting sulfapyridine with nitrous acid and salicylic acid in alkaline media [14, 15]. On the other hand, both phenolic and carboxylic (OH) groups are considered as good coordination sites.

In the present work, several transition metal complexes depending on drugs as potential ligands have been prepared, it is suggested that the sulfasalazine ligand act as bidentate ligand and coordination with metal occurs through the both phenolic and carboxylic (OH) groups. Examining the synthesis, characterization, spectral, thermal, and biological activity studies of sulfasalazine and its metal complexes is the primary focus of this article.

2. Experimental

2.1. Chemicals and synthesis procedure

All of the chemicals were of analytical grade, obtained from Sigma Aldrich and Merck companies, and utilized exactly as supplied without additional purification.

The synthesis procedure of SSZ simple metal complexes was carried out by the addition of a hot methanolic solution (60 ^{o}C) of the appropriate hydrated metal chloride of Cr(III), Mn (II), Fe(III), Co(II), Ni(II) and Cu(II) ions (25 mL, 0.1 mmol) to a hot ammoniacal methanolic solution of sulfasalazine (25 mL, 0.1 mmol) with stoichiometry, 1 :1 (M : L). The mixture was stirred for 1 hour and left in the refrigerator overnight whereby the complexes were precipitated. The isolated complexes were filtered, washed thoroughly with methanol and then with diethyl ether. The solid

complexes were dried in a vacuum desiccator over anhydrous calcium chloride. Two mixed sulfasalazine metal complexes of (Cu(II), Ni(II)) and(Cu(II), Zn(II)) were synthesized with the previously mentioned procedure but with different molar ratio (1:2:2) (M1: M2: L) by mixing methanolic solutions of both hydrated metal chloride together and then addition to hot ammoniacal methanolic solution of sulfasalazine.

It was reported that sulfasalazine has four ionization constants [16], corresponding to the deprotonation of the protonated pyridine nitrogen, carboxylic OH, phenolic OH and sulfonamide hydrogen, respectively. 0.62, 2.9, 8.7 and 11.1, the free carboxylic form of sulfasalazine is insoluble in water and very slightly soluble in ethanol and methanol so that pH of the solution was adjusted to (8.0 –9.0) with 0.1 M NH_4OH solution in which the carboxylic acid group is ionized.

Elemental analysis, melting point, formula, molecular weight, stoichiometries and colour of the complexes are given in Table 1.

2.2. Physical measurements

a) Metal ion content: Atomic absorption technique using (Shimadzu-atomic absorption spectrophotometer, model AA-6650) used for metal content determination.

b) C, H, N, S and Cl contents: Carbon, hydrogen, nitrogen and sulfur for s all synthesized complexes were recorded on Automatic CHNS (Vario EL III Germany) contents of all the synthesized complexes were analyzed by the usual method [17]. The well-known Volhard method was used in acidic medium to analyze the chloride content of complexes [18].

c) Infrared spectra (IR): The infrared spectra of sulfasalazine and its metal complexes were taken in potassium bromide disc using Perkin Elmer spectrophotometer, Model 1430 covering frequency range of 200- 4000 cm^{-1}.

d) Electronic spectra (UV-Vis): The spectra of the solid colored complexes were measured in nujol mull spectra, following the method described by Lee, Griswold and Kleinberg [19] using Ultraviolet Shimadzu– 1650 PC, covering the wave length range 190 $^{-1}$100 nm.

e) Magnetic susceptibility: Magnetic susceptibility measured at 32.5 ^{o}C on Sherwood Scientific Magnetic susceptibility balance (Cambridge, UK) (using Evans method. Diamagnetic corrections were calculated using Pascal's constants [20]. $Hg[Co(SCN)_4]$ was used as calibrant. The values of effective magnetic moments were calculated from the following equation μeff = 2.828 (XMcorrt T)1/2, where XMcorrt is the molar magnetic susceptibility corrected for diamagnetism of all atoms in the compounds.

f) Electron spin resonance spectra (ESR): EPR measurements were performed using X-band EPR spectrometer (Bruker EMX, Germany) at room temperature using a high-sensitive standard cylindrical resonator (ER4119HS) operating at 9.85 GHz, with a 100 kHz modulation frequency. The (g) values were determined by comparison with (2, 2-diphenyl picryl hydrazide) DPPH signal (g=2.0037) [21].

g) Fast atom bombardment (FAB) Mass spectrum: Mass spectra for some compounds were recorded on Shimadzu QP-2010 plus

h) The powder X-ray diffraction: The identification of crystal phase of metal complexes was acquired using Bruker MeaSrv (D2-208219) X-ray diffractometer with Cu Kα radiation tube (λ = 1.5406 Å) operating at a voltage of 30 kV, an electric current of 10 mA and scanned between 2θ angular range of 2° to 100° at a scan speed of 0.02°/S with lynxeye type detector.

i) Thermal analysis: Differential thermal analysis (DTA) and thermogravimetric analysis (TG) of sulfasalazine and its complexes were carried out using (Shimadzu DTG-60H). The rate of heating was 10 °C/min. The cell used was platinum and the atmospheric nitrogen rate flow was 15 ml/ min.

2.3. Biological evaluation

a) The antimicrobial activities of sulfasalazine and its metal complexes were examined by using (Agar well diffusion method). The bacterial indicators were: Staphylococcus aureas (ATCC 6538P), Bacillus subtilis (ATCC 19659); (Gram positive), Escherichia Coli (ATCC 8739) strain [22] and Pesudomonas aeruginosa (ATCC 9027)

(Gram negative) and one fungal species Candida albicans (ATCC 2091). Incubation at 37°C for 24 h was required for bacterial cultures; meanwhile fungal cultures were incubated at (25-30°C) for 3-7 days [23].

b) The minimum inhibitory concentration (MIC): measure the lowest concentration required for microbial growth inhibition.

2.4 Molecular docking

The simulated interaction of designed drug with the protein structure of selected pathogens was modeled by MOE2015.10 program. The 3D crystal structure of the selected proteins (6XXO) was obtained from the Protein Data Bank (PDB). The inhibition efficiency of the designed drugs is evaluated by the strength of interactions with the target proteins, which was predicted from the scoring energy and the length of the H-bonds in the docked complex [24, 25].

Table 1: Elemental analysis, m.p, formula, molecular weight, stoichiometries and colour of sulfasalazine metal complexes.

*Mercury metal% is calculated relative to species with similar environment (Zn & Cd).

Complexes	Color	Melting point	Empirical Formula M.Wt (g/mol)	Elemental analysis, Calculated/ (found)%					
				C%	H%	N%	S%	M%	Cl%
[Zn (SSZ) $(H_2O)_4]\cdot 3H_2O$ (1: 1)	Orange	240	$C_{18}H_{26}N_4O_{12}SZn$ 587.86	36.78 (36.62)	4.46 (4.40)	9.53 (9.62)	5.45 (5.36)	11.12 (11.04)	--------
[Cd (SSZ) $(H_2O)_4]\cdot 2H_2O$ (1: 1)	Yellow	228	$C_{18}H_{24}CdN_4O_{11}S$ 616.88	35.05 (34.95)	3.92 (3.84)	9.08 (9.22)	5.20 (5.33)	18.22 (18.35)	---------
[Hg (SSZ) $(H_2O)_4]\cdot 3H_2O$ (1: 1)	Yellow	212	$C_{18}H_{26}HgN_4O_{12}S$ 723.07	29.90 (29.63)	3.62 (3.54)	7.75 (7.65)	4.43 (4.62)	(26.55)*	---------
$[Cu_2$ Ni $(SSZ)_2$ $(H_2O)_4Cl_4]\cdot 6H_2O$ (2:1: 2)	Dark brown	305	$C_{36}H_{46}Cl_4Cu_2N_8NiO_{20}S_2$ 1302.51	33.20 (32.92)	3.56 (3.54)	8.60 (8.43)	4.92 (5.17)	Cu 9.76 (9.82) Ni 4.51 (4.64)	10.89 (10.62)
$[Cu_2Zn(SSZ)_2$ $(H_2O)_4Cl_4]\cdot 5H_2O$ (2:1: 2)	Brown	299	$C_{36}H_{44}Cl_4Cu_2N_8O_{19}S_2Zn$ 1291.18	33.49 (33.13)	3.44 (3.58)	8.68 (8.79)	4.97 (5.07)	Cu 9.84 (10.25) Zn 5.06 (5.12)	10.98 (10.74)

*All melting points pointed to starting fusion since the complexes take a range from 4 to 5 oC range to be fused completely.

3. Results and Discussion

3.1. Infrared spectral studies of sulfasalazine and its complexes:

The IR spectra obtained for the complexes, Figure (2, 3), were analyzed in comparison to the spectrum of the ligand. Absorption in the (4000–2600 cm^{-1}) region involves the bands of –OH, –NH and SO_3H groups as well as those of the C–H phenyl, C–H aliphatic and associated water molecules in the complexes. IR spectrum of the free sulfasalazine showed a medium broad band at 3405cm^{-1}, which was attributed to the phenolic OH and carboxylic OH groups, (O–H) stretching band indicating overlapping of the peaks due to the (C–H) structure of aryl group and(C–H) stretching of methyl group peaks have appeared as shoulders between 2825cm^{-1} to 2919cm^{-1}.

As the ammonium salt of sulfasalazine is used in the preparation of complexes, the stretching vibration of the carboxylic OH is no longer to be considered in the prepared complexes. In addition, the existence of water of hydration and/or water of coordination in the spectra of the complexes rendered it difficult to get conclusion from the changes expected to the vibration of the phenolic OH group.

Generally, Sulfasalazine metal complexes IR spectra, Table (2), show abroad diffuse band with strong-to-medium strong intensity in the (3340– 3534 cm^{-1}) region may be assigned to the OH stretching vibration for the coordinated water molecules in all prepared complexes and γ(OH) in the range (909 –969 cm^{-1}) suggesting coordination with water. It seems from the elemental analysis of the complexes and thermal analysis that all complexes contain water molecules in their structures. This is evident by νOH, Table (2). However, coordinated water in these complexes is indicated by the appearance of metal-oxygen bands attributable to rocking modes at (414- 498 cm^{-1}) region [26].

The essential region1700–1200 cm^{-1} in the infrared spectra is interesting, since it contains bands of carboxylate (COO^{-} stretching bands), phenolic C– O, azo N=N–, C=N and C=C.

The carboxylate ion usually coordinates to metal ions in three main ways. The values of Δν = νasym(COO) – νsym(COO) with a high probability in monodentate complexes are expected to be much larger than 200 cm^{-1}, or much greater than the ionic complexes. In most cases, complexes with Δν < 200, have chelating and/or bridging carboxylate groups [27-29]. All the prepared complexes IR spectra have Δν greater than 200 cm^{-1}, the asymmetric CO_2 fall in the range (1622-1632 cm^{-1}), the symmetric CO_2 stretches also fall in (1414-1421 cm^{-1}). which confirm the monodentate nature of caraboxylate group.

To ascertain the involvement of ν(OH) of phenolic group of sulfasalazine in the coordination process a follow up of the stretching vibration bands of(C–O) in SSZ complexes is required and found that the ν(C–O) shifted to lower wave number from 1261cm^{-1} in case of free ligand to (1246 to 1252cm^{-1}) in case of metal complexes. This result indicates that the phenolic group participated in the complexation and the SSZ ligand acted as bidentate. The phenolic OH was found deprotonated in the complexes, which was apparent from the absence of the ν(OH) in-plane bending (1394 cm^{-1}) in the free SSZ ligand [30].

The other ligand vibrations like aromatic (C=C), (C=N) of pyridine ring, (–N=N–) and (O=S=O) show bands around 1600 cm^{-1} for skeleton of the benzene ring (C=C vibration) of the free ligand which always interferes with the other bending vibration of the water molecule δ(OH) in the prepared complexes. The bands at 1535 cm^{-1} for (C=N), 1465 cm^{-1} described azo bond vibrational mode (–N=N–) and 1359, 1173 cm^{-1} for asymmetric and symmetric (O=S=O) vibrations respectively, these vibrations remained unchanged or slightly shifted in metal complexes, which may be attributed to the electronic density changes on these groups after complex formation [31].

The participation of the phenolic and carboxylic group was also confirmed by the appearance of new bands in the complexes confirmed by the appearance of new bands in the complexes in the 414–498 cm^{-1} regions, which were assigned to the ν (M–O) stretching vibrations [32].

3.2. Electronic absorption spectra and magnetic susceptibility studies

The UV-Vis spectra of sulfasalazine ligand and its complexes in DMSO exhibit and detect peaks which are tabulated in, Table (3) and Figure (4). The UV-Vis spectra for free ligand sulfasalazine revealed two absorption maxima peaks at 255, 355 assigned to π–π* and n→ π* transitions within the organic moiety of the ligand. Throughout complexation, these bands may get weaker or disappear.

A. Zn, Cd and Hg-complexes

The orange [Zn (SSZ) $(H_2O)_4$].$3H_2O$ and the yellow [Cd (SSZ) $(H_2O)_4$].$2H_2O$, [Hg (SSZ) $(H_2O)_4$].$3H_2O$ complexes were found to be diamagnetic with effective magnetic moment (μeff) equal zero, as a consequence of the d_{10} configuration of Zn(II) ,Cd (II), Hg (II) no d-d transition could be observed , so it is impossible to deduce from ultraviolet and visible spectra the stereochemistry surrounding these metals in their complexes .

These complexes exhibited a high intensity bands at 285-420 nm, which are attributed to ligand → metal charge transfer. The complexes' proposed geometry is based on bidentate nature of sulfasalazine ligand and four water molecules in the inner sphere. However, by comparing the spectra of these complexes and those of similar environments, an octahedral geometry are suggested for these complexes as shown in the Figures (4) [33 -35].

B. Mixed metal complexes:

The dark brown Cu-Ni complex with the formula $[Cu_2\ Ni\ (SSZ)_2\ (H_2O)_4Cl_4].6H_2O$ showed bands at λ_{max} 320, 455, 505, 640 and 789 nm the first one is due to charge transfer, thus the visible d-d electronic spectral band at 505 nm may probably be due to square planner configuration around Ni (II) [36] , since the ESR data identified axial compressed spectrum for mixed Cu-Ni sulfasalazine complex combined with the appearance of three visible bands assume distorted octahedral geometry around Cu (II) ion. Such finding gathered with room temperature effective magnetic moment value of the complex (μ_{eff} = 3.32 B.M) pointed to its existence of distorted octahedral configuration for Cu (III) and square planar configuration for Ni (II).

Table 2: Fundamental infrared bands (cm^{-1}) of sulfasalazine (SSZ) and its metal complexes.

Compound	ν (O-H) (H_2O)	γ (OH) (H_2O)	ν COO (asymm)	νCOO (symm)	Δν (COO)	ν SO_2 (asymm)	ν SO_2 (symm)	ν (C-O)	ν (N=N)	ν (C=N)	ν (M -O)	ν (M –Cl)
Sulfasalazine	-------	------	1676	1427	------	1359	1173	1261	1465	1535	-----	-----
[Zn (SSZ) $(H_2O)_4$] $.3H_2O$ (1: 1)	3452	959	1625	1421	204	1359	1174	1248	1465	1534	475	-----
[Cd (SSZ) $(H_2O)_4$] $.2H_2O$ (1: 1)	3539	966	1626	1417	209	1358	1173	1252	1467	1533	414	------
[Hg (SSZ) $(H_2O)_4$] $.3H_2O$ (1: 1)	3534	964	1629	1416	215	1359	1171	1247	1466	1537	456	------
$[Cu_2$ Ni $(SSZ)_2$ $(H_2O)_4Cl_4]$ $.6H_2O$ (2:1: 2)	3498	948	1631	1417	214	1358	1173	1251	1464	1532	482	347
$[Cu_2Zn(SSZ)_2$ $(H_2O)_4Cl_4]$ $.5H_2O$ (2:1: 2)	3477	946	1630	1414	216	1357	1172	1249	1465	1535	475	365

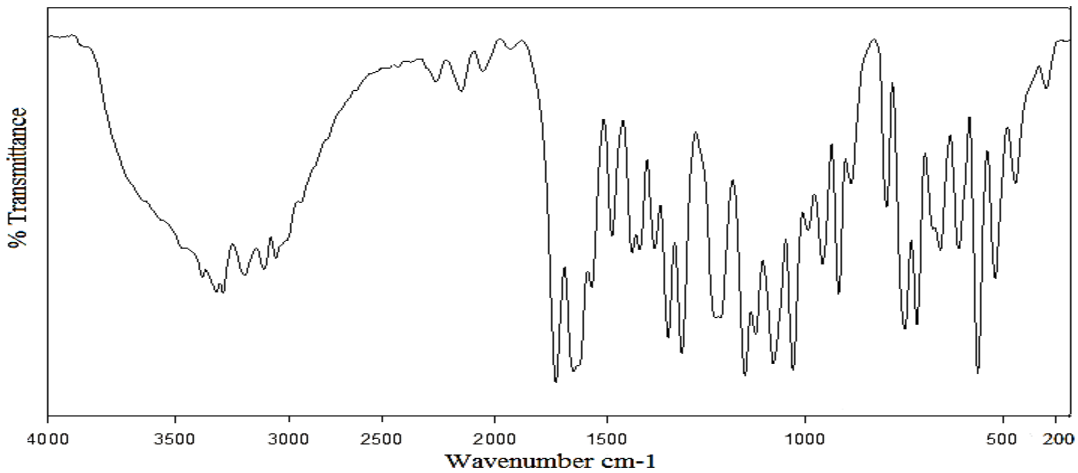

Figure 2: Infrared spectrum of sulfasalazine ligand

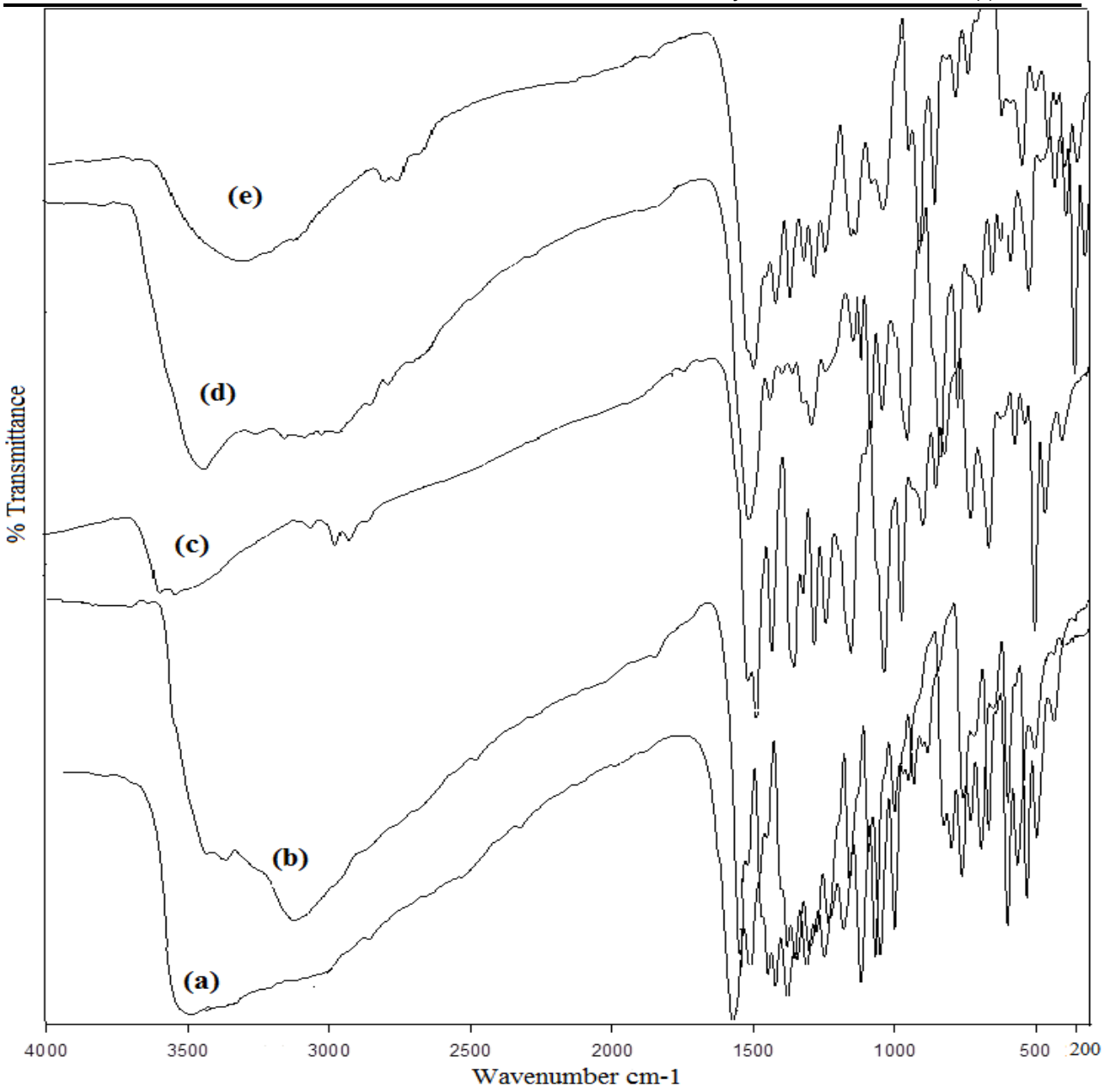

Figure 3: Infrared spectra of some sulfasalazine metal complexes (a) [Zn (SSZ) $(H_2O)_4$] .$3H_2O$, (b) [Cd (SSZ) $(H_2O)_4$] .$2H_2O$, (c) [Hg (SSZ) $(H_2O)_4$] .$3H_2O$, (d) [Cu_2 Ni $(SSZ)_2$ $(H_2O)_4Cl_4$] .$6H_2O$, (e) [$Cu_2Zn(SSZ)_2$ $(H_2O)_4Cl_4$].$5H_2O$.

Moreover, the mixed metal complex derived from $CuCl_2$ and $ZnCl_2$ with sulfasalazine could be formulated [$Cu_2Zn(SSZ)_2$ $(H_2O)_4Cl_4$] .$5H_2O$ gave four bands at 312 460, 605 and 820 nm, Figure (4) and Table (3), the first band is due to charge transfer ,the three visible band may attributed to distorted octahedral geometry of Cu , Zn has no visible band due to d10 configuration ,no d-d transition could be observed. Such finding gathered with room temperature effective magnetic moment value of the complex (μeff = 3.4 B.M) pointed to its existence of distorted octahedral configuration for Cu (III) and tetrahedral configuration for Zn (II) [37].

Table 3: Nujol mull electronic absorption spectra (nm, cm $^{-1}$), room temperature magnetic moment values (μ_{eff}, 298°K) B.M, of some sulfasalazine metal complexes.

Complex	**Color**	**UV bands (cm^{-1}) nm**		**Band assignment**	**Magnetic moment μ_{eff} (B.M)**	**Geometry**
[Zn (SSZ) $(H_2O)_4$] $.3H_2O$ (1: 1)	Orang	ν_2	31746 315	CT	Zero	O_h
		ν_1	24691 405			
[Cd (SSZ) $(H_2O)_4$]. $2H_2O$ (1: 1)	Yellow	ν_2	33444 299	CT	Zero	O_h
		ν_1	24271 412			
[Hg (SSZ) $(H_2O)_4$] $.3H_2O$ (1: 1)	Yellow	ν_2	35087 285	CT	Zero	O_h
		ν_1	23809 420			
[Cu_2 Ni $(SSZ)_2$ $(H_2O)_4Cl_4$] $.6H_2O$ (2:1: 2)	Dark Brown	ν_5	31250 320	CT	3.32	Cu O_h Ni S.P
		ν_4	21978 455	$^2B_{1g} \rightarrow {}^2E_g$		
		ν_3	19801 505	$^1A_{ig} \rightarrow {}^1A_{2g}$ and $^1A_{ig} \rightarrow {}^1B_{1g}$		
[$Cu_2Zn(SSZ)_2$ $(H_2O)_4Cl_4$] $.5H_2O$ (2:1: 2)	Brown	ν_2	15625 640	$^2B_{1g} \rightarrow {}^2B_{2g}$	3.4	Cu O_h Zn Td
		ν_1	12674 789	$^2B_{1g} \rightarrow {}^2A_{1g}$		
		ν_4	32051 312	CT		
		ν_3	21739 460	$^2B_{1g} \rightarrow {}^2E_g$		
		ν_2	16528 605	$^2B_{1g} \rightarrow {}^2B_{2g}$		
		ν_1	12195 820	$^2B_{1g} \rightarrow {}^2A_{1g}$		

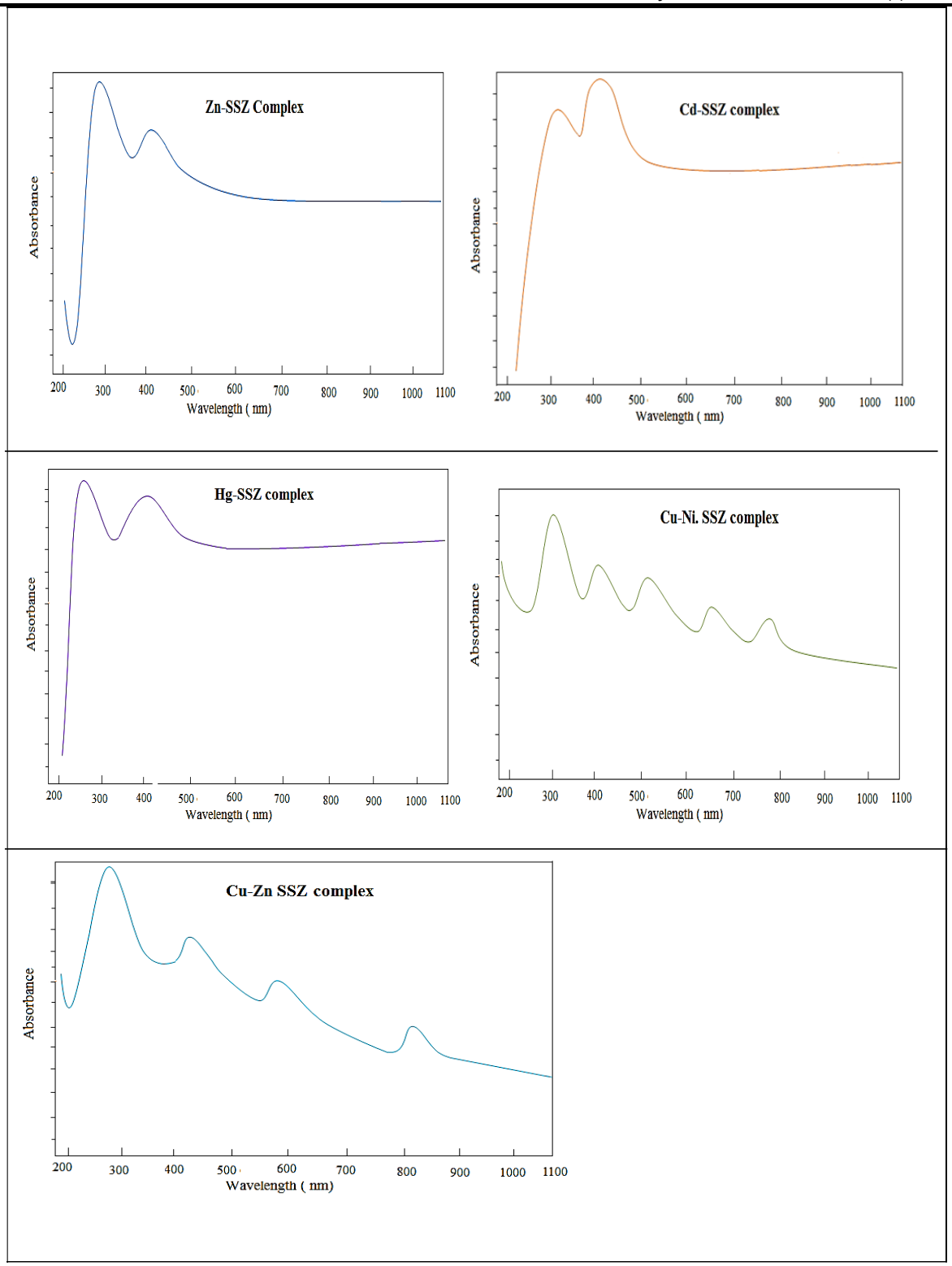

Figure 4: Nujol mull electronic absorption spectra of some sulfasalazine metal complexes (Zn, Cd, Hg, Cu-Ni, and Cu-Zn)

3.3. Electron spin resonance

3.3.1. Electron spin resonance mixed copper complexes

The room temperature polycrystalline X-band ESR spectral pattern of mixed copper complexes $[Cu_2Ni(SSZ)_2(H_2O)_4Cl_4].6H_2O$ and $[Cu_2Zn(SSZ)_2(H_2O)_4Cl_4].5H_2O$, Figure (5, 6) and Table (4), are nearly of similar pattern. Both are anisotropic in nature where $g_{\shortparallel} = 2.045$ and 2.025 and $g\perp = 2.260$ and 2.263 respectively.

The < g> values were calculated from the equation $g_{av} = 1/3(g_{\shortparallel} + 2\, g\perp)$ to be 2.188 and 2.183 respectively for the two complexes .The g values that were found to be more than 2.000 indicated the d_{z2} ground state rather than $d_{x2} - y_2$. The values of $A_{\shortparallel}$ = 235.29 and 242.64 (x 10-4) cm^{-1} respectively.

These $A_{\shortparallel}$ values which are more than 100(x 10^{-4}) cm^{-1} prevent the pseudo tetrahedral structure around the copper atoms, indicating Oh geometry around copper atoms in the studied complexes.

The G values were 0.173 and 0.0943 to both Cu complexes, as G is less than 4 this indicated the presence of very strong interaction between copper atoms in the solid state [38, 39].

This data revealed that both complexes were axially compressed. Such findings correlate with the magnetic properties that have already been discussed. The values of α^2 parameter for $[Cu_2Ni(SSZ)_2(H_2O)_4Cl_4].6H_2O$ and $[Cu_2Zn(SSZ)_2(H_2O)_4Cl_4].5H_2O$ were found to be 0.847 and 0.848 and – metal bonds assigned that Cu-O bond is more pronounced for complexation .The f^2 values which are the fraction of the 3d character in the Cu^{II} 3d-4S ground state were found to be 0.74 and 0.73 respectively.

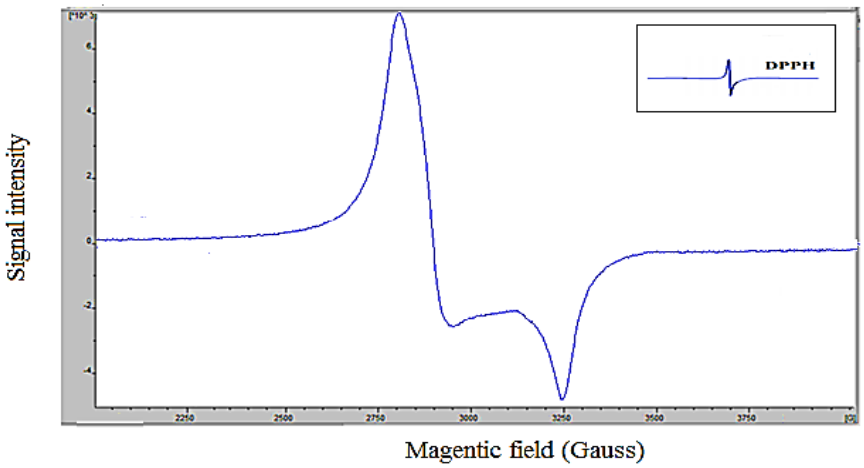

Figure 5: ESR spectrum of $[Cu_2 Ni (SSZ)_2 (H_2O)_4Cl_4] .6H_2O$ complex.

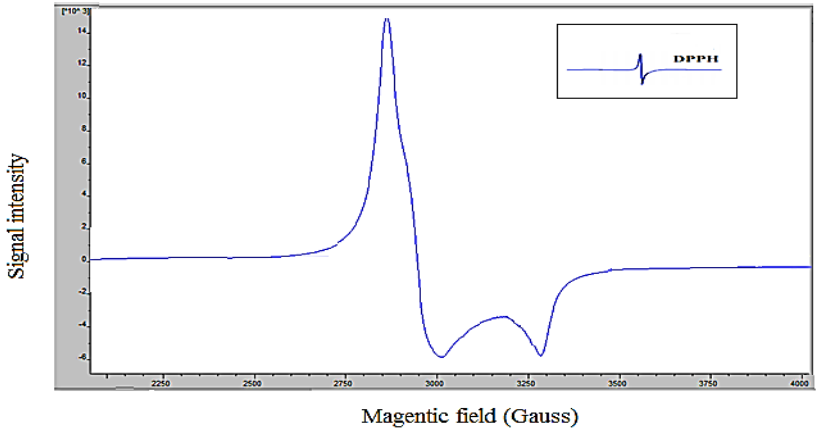

Figure 6: ESR spectrum of $[Cu_2Zn(SSZ)_2 (H_2O)_4Cl_4] .5H_2O$ complex

Table (4): Room temperature ESR spectral parameters of mixed sulfasalazine copper complexes.

Complex	g_{II}	$g_{\perp}$	<g>	$A_{II}.10^{-4}$	G	α^2	f^2	g_{II}/A_{II}	|A|
$[Cu_2 Ni (SSZ)_2 (H_2O)_4Cl_4] .6H_2O$	2.045	2.260	2.188	235.29	0.174	0.847	0.743	86.91	94.12
$[Cu_2Zn(SSZ)_2 (H_2O)_4Cl_4] .5H_2O$	2.025	2.263	2.183	242.64	0.094	0.848	0.739	83.45	97.06

3.4 Mass spectra of sulfasalazine ligand and Cd(II) Complex:

The mass spectrum of sulfasalazine ligand (SSZ) revealed an exact parent molecular ion peak at m/z 398.07 a.m.u which corresponding to the theoretical molecular weight ,in addition various peaks showed in the mass spectrum with relative intensities ,peaks observed at m/z 398.07, 381.07, 332.09, 317.10, 315.09, 242.07, 165.03, 137.02 and 94.05 a.m.u representing M^+, $[C_{18}H_{13}N_4O_4S]^+$, $[C_{18}H_{12}N_4O_3]^+$, $[C_{18}H_{13}N_4O_2]^+$, $[C_{18}H_{11}N_4O_2]^+$, $[C_{13}H_{10}N_2O_3]^+$, $[C_7H_5N_2O_3]^+$, $[C_7H_5O_3]^+$ and$[C_5H_6N_2]^+$ respectively [40-42].

The peak at 381.07 a.m.u has a higher intensity and indicates the very stable charged ion in ligand structure (base peak). The fragments, their molecular weight and relative intensity (%) are ordered, Table (5), Figure (7).

In order to demonstrate the differences in the fragmentation pathway for the free ligand (SSZ) and the impact of metal ions after complexation, mass spectra for the free ligand and [Cd (SSZ) $(H_2O)_4$]. $2H_2O$ complex, Figure (8), have been utilized; this difference proves the existence of complexation process.

The analysis of [Cd (SSZ) $(H_2O)_4$]. $2H_2O$ by mass spectrometry is a powerful method for determining molecular weight. Moreover, it provides data on the mechanism of fragmentation, in the mass spectrum of [Cd (SSZ) $(H_2O)_4$]. $2H_2O$, Figure (8), a peak recorded at m/z = 580.21which attributed to the mass of the complex and also confirm 1:1 (M :L) composition, also the spectrum showed abase peak with greatest intensity at m/z = 93.65 corresponding to the more stable fragment.

Table 5: Mass spectrum fragmentations of sulfasalazine ligand

Assignment	Molecular weight	m/z	Relative abundance
M^+	398.39	398.07	7.5
$[C_{18}H_{13}N_4O_4S]^+$	381.39	381.07	100
$[C_{18}H_{12}N_4O_3]^+$	332.32	332.09	5.6
$[C_{18}H_{13}N_4O_2]^+$	317.33	317.10	20.35
$[C_{18}H_{11}N_4O_2]^+$	315.31	315.09	3.4
$[C_{13}H_{10}N_2O_3]^+$	242.23	242.07	45.07
$[C_7H_5N_2O_3]^+$	165.13	165.03	10.4
$[C_7H_5O_3]^+$	137.11	137.02	17.5
$[C_5H_6N_2]^+$	94.12	94.05	6.2

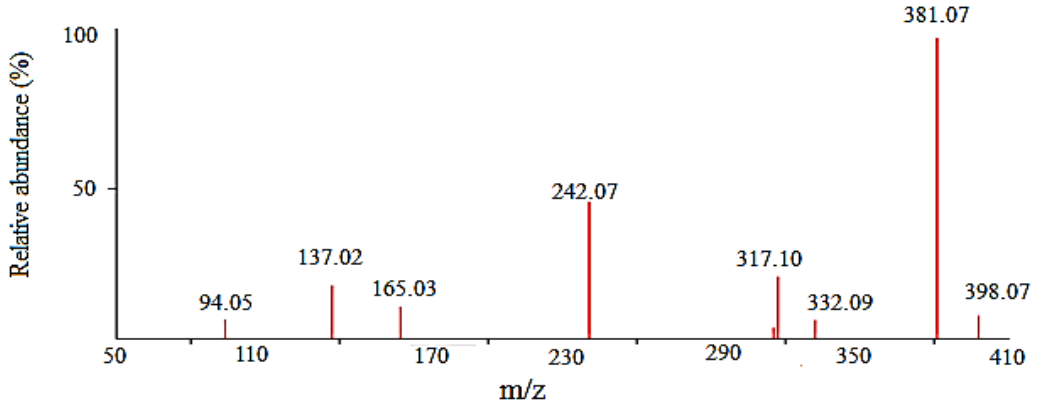

Figure 7: Mass spectrum of sulfasalazine ligand

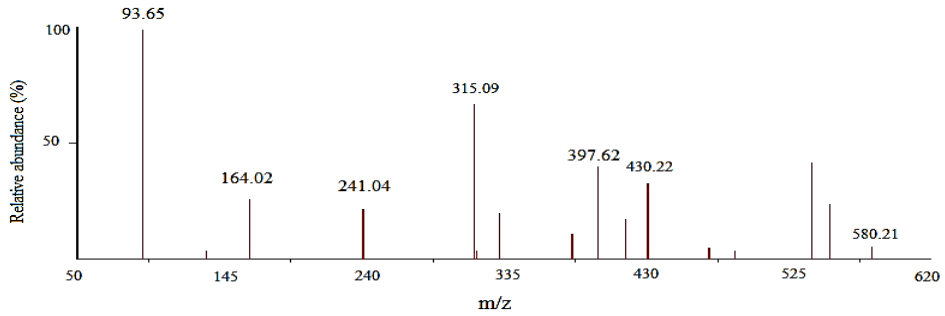

Figure 8: Mass spectrum of [Cd (SSZ) $(H_2O)_4$]. $2H_2O$ complex

From Elemental analysis, IR, electronic absorption spectra, magnetic moment values, mass spectra and ESR, structures of metal complexes were elucidated according to shown in:

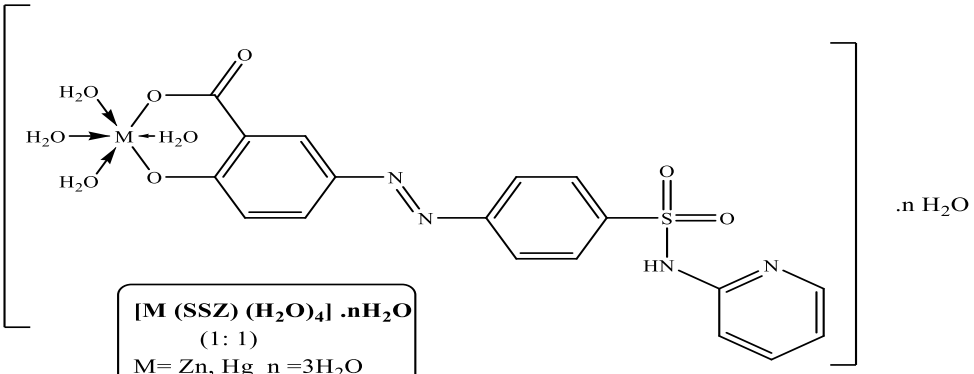

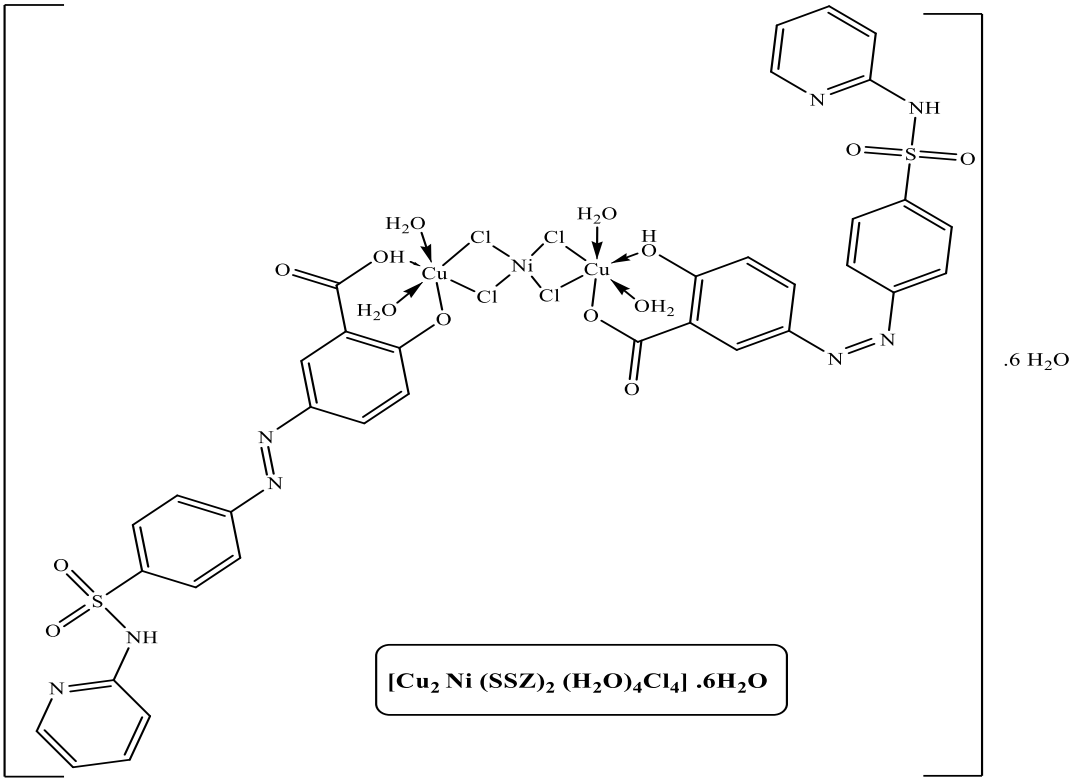

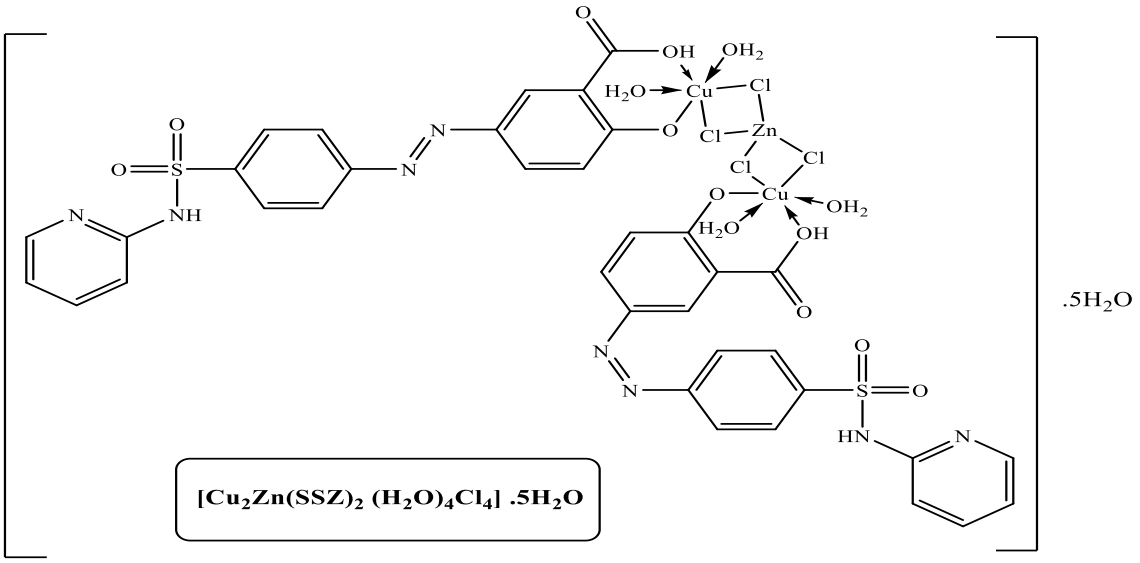

Figure 9: Proposed structure of some sulfasalazine complexes

3.5. The powder X-ray diffraction (PXRD)

The most accurate way to study a complex's structure is through single crystal X-ray crystallography, but because it can be challenging to obtain crystalline complexes in a properly symmetric form, powder X-ray diffraction is used to learn more about the structure and clarify the binding site of the ligand that chelated with the metal in prepared complexes like [Cd (SSZ) $(H_2O)_4$]. $2H_2O$, [Hg (SSZ) $(H_2O)_4$] .$3H_2O$.

Powder XRD patterns of [Cd (SSZ) $(H_2O)_4$]. $2H_2O$, [Hg (SSZ) $(H_2O)_4$] .$3H_2O$. recorded in the range (2Θ = 0 –100) was shown in Figure (10,11), XRD pattern of the metal complex exhibited sharp crystalline peaks indicating its crystalline phase, Crystalline material or crystal is atoms are arranged in aperiodic pattern of three dimension. Not all solids are crystalline; however some solids don't possess any regular interior arrangement of atoms called amorphous such as glass [43].

The average crystallite size (dXRD) of the complexes was calculated using Scherer's formula: $D = K\lambda / \beta \cos\theta$, Where , K=0.9 (Scherrer constant) λ(wavelength) = 0.15406 nm, β= FWHM (radians) and Θ is the Bragg angle (peak position in radians). The peak width β in radians (often measured as full width at half maximum, FWHM) is inversely proportional to the crystallite size (D) (Whilst small crystals are the most common cause of line broadening but other defects can also cause peak widths to increase) [44,45]. The results of X-ray diffraction of [Cd (SSZ) $(H_2O)_4$]. $2H_2O$, [Hg (SSZ) $(H_2O)_4$] .$3H_2O$, Figure (10,11), plot the intensity of the signal for various angles of diffraction at their respective two theta positions, the plotted data smoothed by origin 2024 software.

The unit-cell parameters for [Cd (SSZ) $(H_2O)_4$] .$2H_2O$ is determined through profile flattering and indexing of X-rary powder diffraction that illustrated a orthorhombic cell with the lattice parameters a= 18.9060 Å, b = 7.9483Å, c = 9.9809 Å, $\alpha = \beta = \gamma = 90^o$ while Z is equal (4) and cell volume is 27.435 nm^3 for [Cd (SSZ) $(H_2O)_4$] .$2H_2O$. complex.

By implementation the (Match V.2) computer software on a PXRD data of [Cd (SSZ) $(H_2O)_4$] .$2H_2O$ and solving the structure which deduced that the most adequate space group for this metal complex is C m c 21 (No.36). Some important parameters such as hkl file data ,2Θ and d that can be obtained by using Rietveld refinements method of the software programe (Match V.2) ,Figure (12).

Mean while, the unit-cell parameters for [Hg (SSZ) $(H_2O)_4$] .$3H_2O$ is determined through profile flattering and indexing of X-rary powder diffraction that illustrated a triclinic cell with the lattice parameters a= 8.1287 Å , b = 9.4916 Å, c = 6.8940 Å, $\alpha = 100.356^o$, $\beta = 110.163^o$, $\gamma = 82.981^o$, while cell volume is 51.051 nm^3 for [Hg (SSZ) $(H_2O)_4$] .$3H_2O$. complex.

By implementation the (Match V.2) computer software on a PXRD data of [Hg (SSZ) $(H_2O)_4$] .$3H_2O$. and solving the structure which deduced that the most adequate space group for this metal complex is P^{-1} (No. 2). Some important parameters such as hkl file data ,2Ɵ and d that can be obtained by using Rietveld refinements method of the software programe (Match V.2), Figure (13).

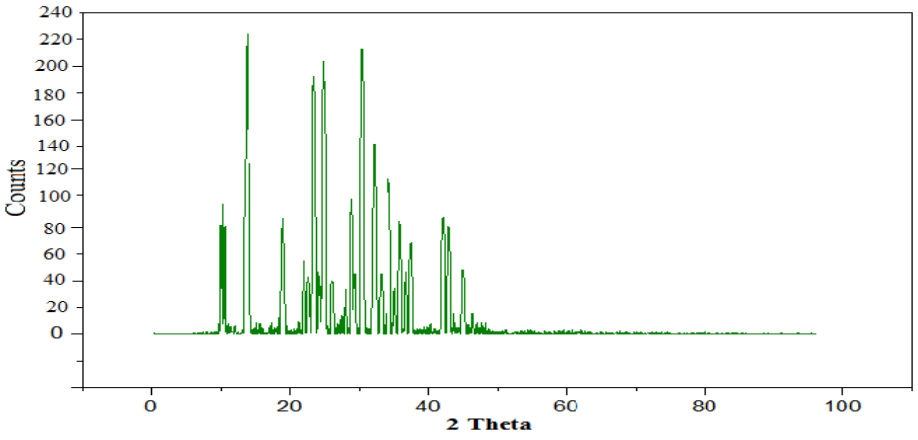

Figure 10: Powder XRD pattern of [Cd (SSZ) $(H_2O)_4$] .$2H_2O$ smoothed by origin2024.

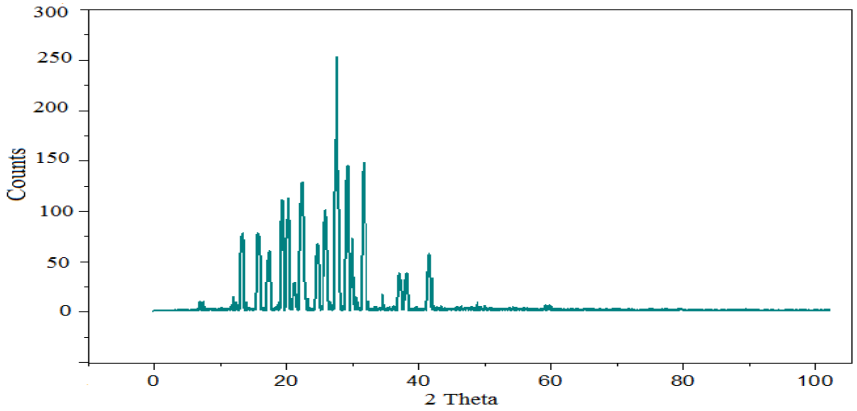

Figure 11: Powder XRD pattern of [Hg (SSZ) $(H_2O)_4$] .$3H_2O$ smoothed by origin 2024.

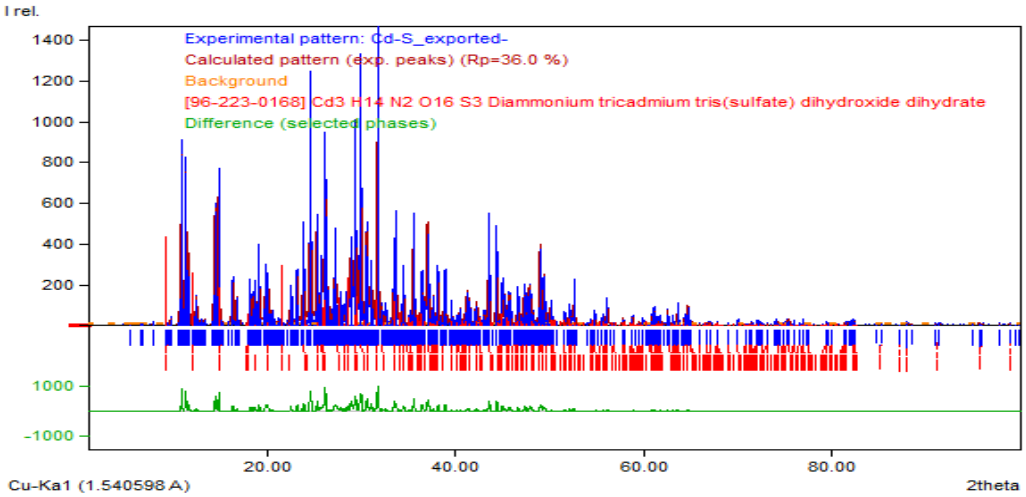

Figure 12: The PXRD graph of [Cd (SSZ) (H2O)$_4$] .$2H_2O$ adjusted by using Rietveld refinement tool.

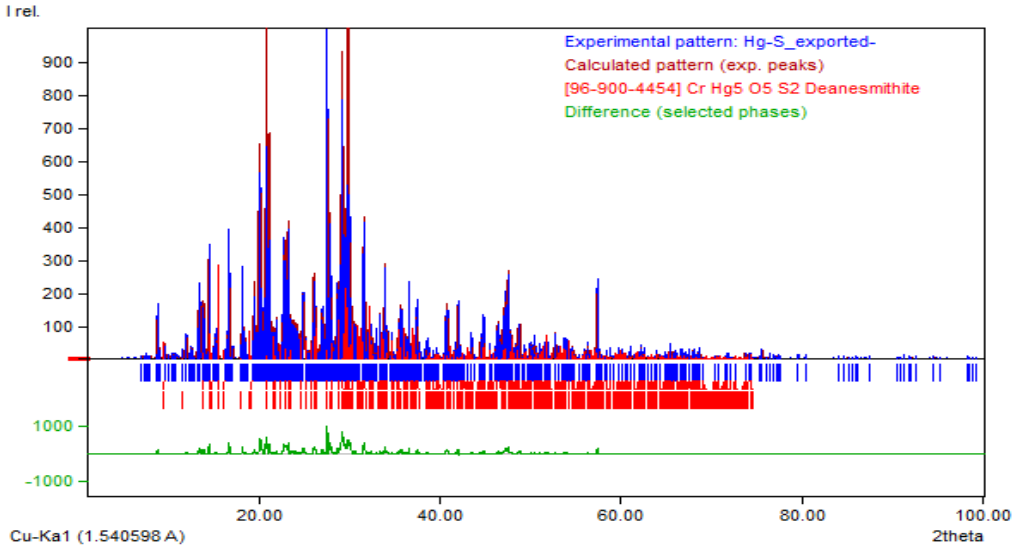

Figure 13: The PXRD graph of [Hg (SSZ) $(H_2O)_4$] .3H_2O adjusted by using Rietveld refinement tool.

3.6. Thermal analysis

From TGA curve sulfasalazine ligand was thermally decomposed in two successive decomposition steps within the temperature range (240 – 560 ºC). The first decomposition step with an estimated mass loss of (46.23%) within the temperature range (240–320 ºC) may be attributed to the liberation of (CH_3OH, NH_3, CO_2, SO_2 and HCN). The second step found within the temperature range (320–560ºC) with an estimated mass loss of 17.58 % which is reasonably accounted for by the removal of (2 NH_3 and 3C) along with the decomposition of the ligand ending with a final residue of (12C).

From DTA curve, Figure (14) and Table (6), the free ligand decomposition occurs in two steps one endothermic at 540 K and the second one is exothermic at 728 K with activation energies 54.59 and 294.82 KJ/mole with orders 1.20, 1.19, respectively. All peaks are of the first order. The mechanism of decomposition could be represented in the following scheme (1):

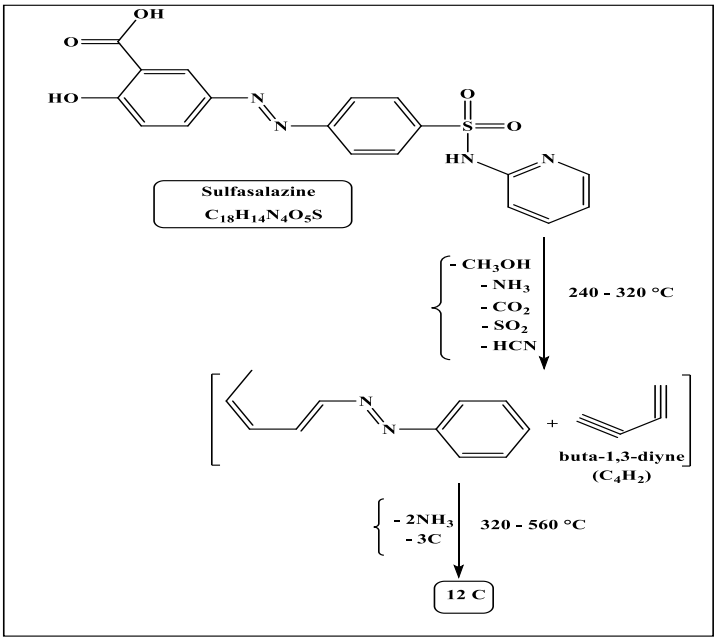

Scheme 1: Proposed thermolysis mechanism of sulfasalazine ligand

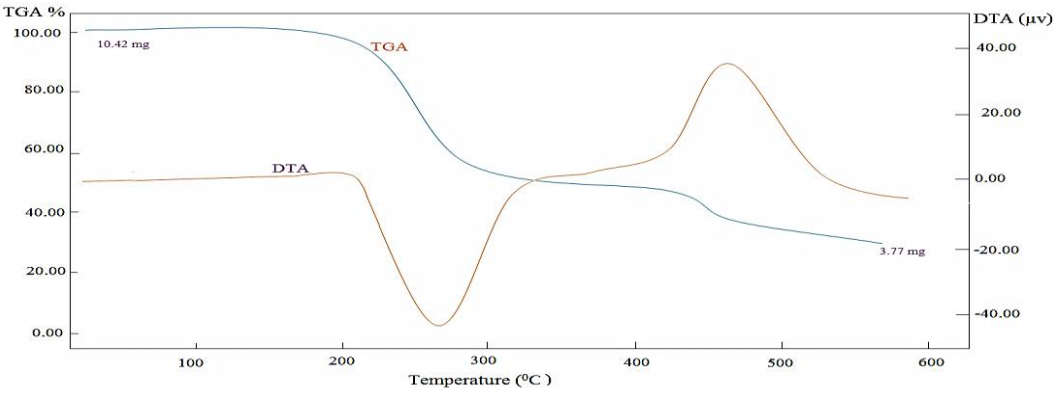

Figure 14: TGA and DTA curves of sulfasalazine ligand

The thermogram of [Cd (SSZ) $(H_2O)_4$] $.2H_2O$ complex gave a decomposition pattern of three stages. The first estimated mass loss of 5.84 % occurs within the temperature range (43.8-154.2 ^oC) and corresponds to the loss of two hydrated water molecules. The subsequent step within the temperature range (154.2-380.8 ^oC) with an estimated mass loss of 22.05% that may be attributed to elimination of ($4H_2O$ and SO_2.), the last stage at temperature range (380.8-599.8 ^oC) with estimated mass loss 47.39% which is reasonably accounted for by decomposition of the ligand ending with a final residue of (CdO+2C). The mechanism of decomposition could be represented in scheme (2).

On the other hand, the DTA data of [Cd (SSZ) $(H_2O)_4$] $.2H_2O$ complex, Figure (15) and Table (6), showed three peaks, at 376, 550 and 740 K with activation energies 51.17, 161.11 and 41.25 kJ/mole, respectively. The orders of reactions were 1.19, 1.50 and 1.54, respectively. All peaks are of the second order type except the first peak is of fist order type. Only the first peak is endothermic type while the other peaks are exothermic types.

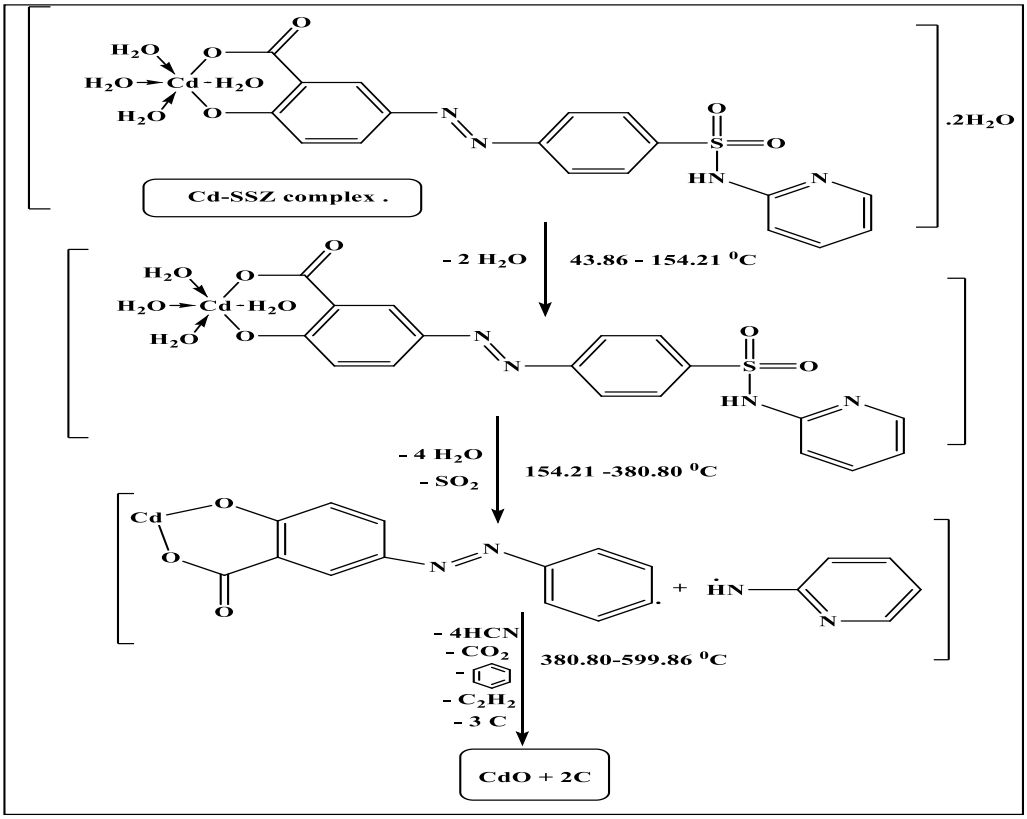

Scheme 2: Proposed thermolysis mechanism of [Cd (SSZ) $(H_2O)_4$] $.2H_2O$ complex.

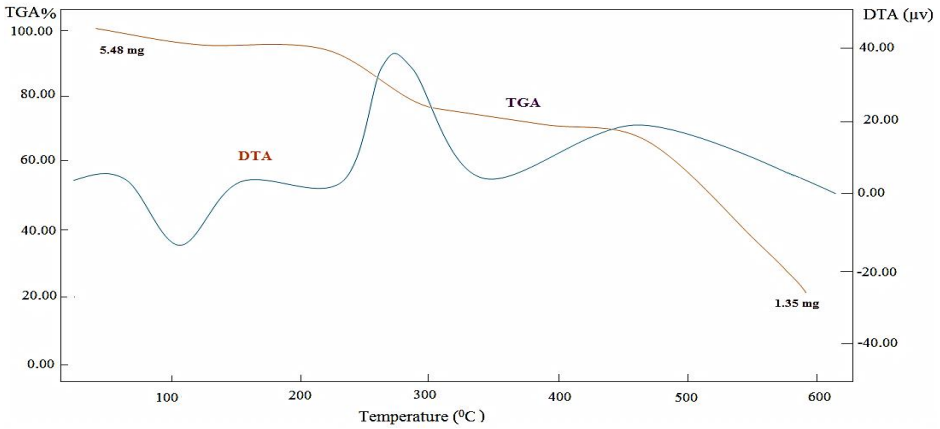

Figure 15: TGA and DTA curves of [Cd (SSZ) $(H_2O)_4$] .$2H_2O$ complex

The TG curve of the $[Cu_2Ni\ (SSZ)_2\ (H_2O)_4Cl_4]\ .6H_2O$ complex, indicated that the complex thermally decomposed in four steps The first estimated mass loss of 13.84% within the temperature range (43.9-122.2 ^oC) may be attributed to loss of ten molecules of water. The second step found in the temperature range (122.2-185.7 ^oC) with an estimated weight loss of 6.76 % corresponds to the loss of ($2NH_3$ and 2HCN).The third step within the temperature range (185.7- 350 ^oC) has estimated mass loss of 18.13% that may be attributed to elimination of ($2SO_2$ and 4HCN) ,The last step with the temperature range (350- 599.2 ^oC) with an estimated mass loss of 33.16 % which is reasonably accounted for by decomposition of the ligand ending with a final residue of (2CuO+NiO+11C)). The mechanism of decomposition could be represented in scheme (3).

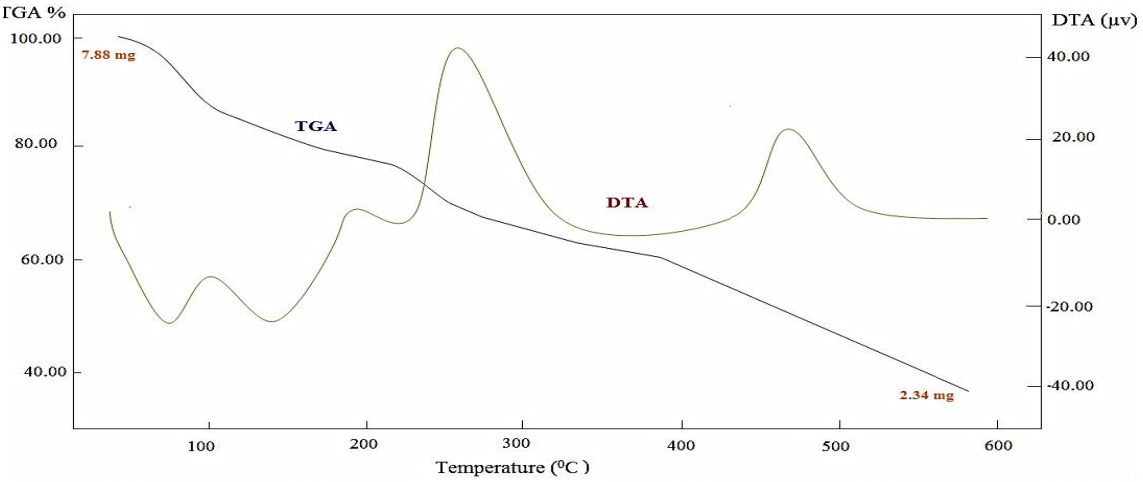

Figure 16: TGA and DTA curves of [Cu_2 Ni $(SSZ)_2$ $(H_2O)_4Cl_4$] .$6H_2O$ complex.

On the other hand, $[Cu_2\ Ni\ (SSZ)_2\ (H_2O)_4Cl_4]\ .6H_2O$ complex, Figure (16) and Table (6), showed four peaks the first two peaks are endothermic while the last two peaks are exothermic at 353, 416, 533 and 748 K, from the DTA data with activation energies of 24.83 ,43.71, 80.59 and 218.92 kJ/mole, their orders of reactions were 1.18 1.12, 1.85, and 1.21, respectively. All the data typified first order reactions except the third peak is of second order type.

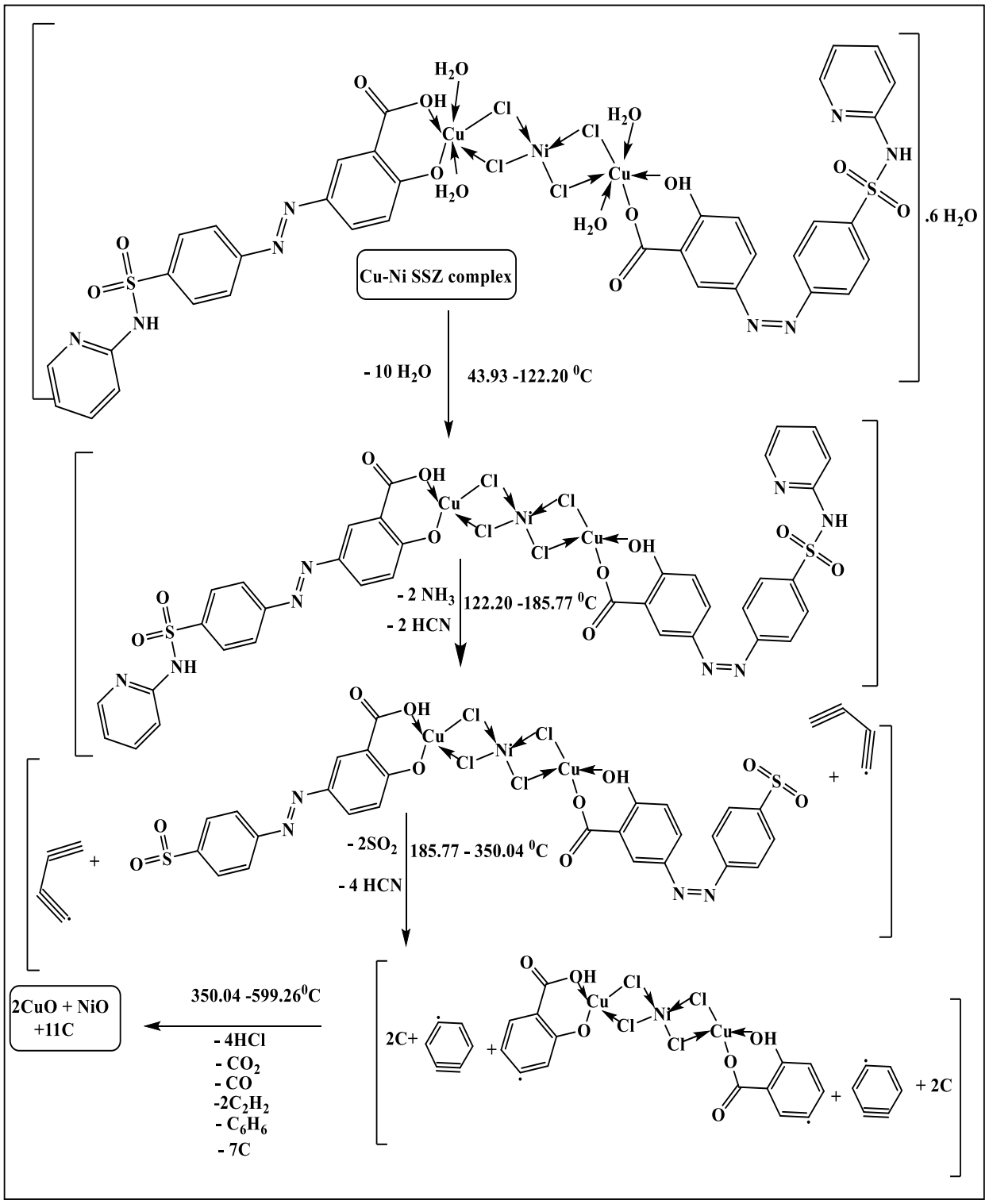

Scheme 3: Proposed thermolysis mechanism of [Cu_2 Ni $(SSZ)_2$ $(H_2O)_4Cl_4$] .6H_2O complex.

Table 6: DTA analysis of some sulfasalazine metal complexes

Compounds	Type	Tm (K)	Ea kJ mol^{-1}	n	α_m	$\Delta S^{\#}$ kJ K^{-1} mol^{-1}	$\Delta H^{\#}$ kJ mol^{-1}	Z S^{-1}	Temp. (°C) TGA	Wt. Loss%		Assignment
										Found	Calc	
Sulfasalazine	Endo	540	54.59	1.20	0.59	-0.31	-165.06	0.012	240-320	46.23	46.11	Elimination of CH_3OH, NH_3, CO_2, SO_2 and HCN
	Exo	728	294.82	1.19	0.60	-0.30	-215.93	0.049	320 -560	17.58	17.65	Loss of 2 NH_3 and 3C
										36.18	36.22	Residue (12C)
[Cd (SSZ) $(H_2O)_4$] $.2H_2O$	Endo	376	51.17	1.19	0.59	-0.30	-112.87	0.016	43.8-154.2	5.84	6.02	Dehydration of $2H_2O$
	Exo	550	161.11	1.50	0.56	-0.30	-163.33	0.035	154.2-380.8	22.05	22.23	Elimination of $4H_2O$ and SO_2.
	Exo	740	41.25	1.54	0.55	-0.31	-231.79	0.007	380.8-599.8	47.39	47.52	Decomposition of the rest ligand and formation of (CdO +2C)
										24.70	24.85	Residue (CdO+2C)
[Cu_2 Ni $(SSZ)_2$ $(H_2O)_4Cl_4$] $.6H_2O$	Endo	353	24.83	1.18	0.60	-0.31	-107.71	0.008	43.9-122.2	13.84	13.92	Dehydration of $10H_2O$
	Endo	416	43.71	1.12	0.61	-0.30	-126.11	0.013	122.2-185.7	6.76	6.85	Elimination of $2NH_3$ and 2HCN.
	Exo	533	80.59	1.85	0.51	-0.30	-161.07	0.018	185.7-350	18.13	18.20	Loss of $2SO_2$ and 4HCN
	Exo	748	218.92	1.21	0.60	-0.30	-224.05	0.035	350-599.2	33.17	32.93	Decomposition of the rest ligand and formation of 2CuO+NiO+11C
										28.08	28.23	Residue(2CuO+NiO+11C)

3.7 Biological evaluation

a) The antimicrobial activities

Sulfasalazine and its metal complexes, Table (7), were found to have antimicrobial activity against five different types of microorganisms representing different microbial categories, Gram positive *(Staphylococcus aureas* (ATCC 6538P)), *(Bacillus subtilis* (ATCC 19659)), Gram negative (*Escherichia Coli* (ATCC 8739) strain and *Pesudomonas aeruginosa* (ATCC 9027)) and one fungal species (*Candida albicans* (ATCC 2091)). The produced compounds' in vitro antibacterial properties were examined as potential growth-inhibiting agents. Using the disc diffusion method, the antibacterial and antifungal screening was done against these five microorganisms. These prepared metal-drug complexes lead to a significant improvement in biological activity compared to the drug itself [47].

To get the necessary test solutions, the compounds were dissolved in DMSO to get the required test solutions.

Using paper disk diffusion method [46], sulfasalazine ligand and its synthesized three simple metal complexes of different metal ions (Zn, Cd and Hg) and two mixed sulfasalazine metal complexes of (Cu(II), Ni(II)) and(Cu(II), Zn(II)) were evaluated for their antimicrobial activities. In this study, the broad range antibiotics ciprofloxacin and clotrimazole are utilized as references. After incubation inhibition of the organisms was evidenced by clear zone surrounding each disk which was measured in millimeters [48-51].

Based on the data shown in Table (7) and Figure (17), the following observations and inferences can be made:

These data clearly indicate that all tested strains were moderately inhibited by the ligand sulfasalazine, while DMSO showed inhibition zone 9 for all microorganisms. However, complexes in comparison to the reference free ligand demonstrate that the coordination of metal ions to bioactive ligands is an interesting strategy that can be further explored, as the complexes exhibited potent anti – microbial effect especially for Gram- positive bacterial strains (*Staphylococcus aureas, Bacillus subtilis*) and fungal strain (*Candida albicans)* but these complexes showed lower efficiency toward Gram negative strains *(Escherichia Coli, Pesudomonas aeruginosa*).

The maximum of inhibition activity (27mm) was observed against (S. aureus) by $[Cu_2Zn(SSZ)_2$ $(H_2O)_4Cl_4]$ $.5H_2O$ complex. It also showed higher activity to *Bacillus subtilis* and *Pesudomonas aeruginosa* . It revealed by the diameter of its inhibition zone which equal 22 and 20 mm respectively. It showed activity in the same range for both *Escherischia coli* and *Candida albicans* with inhibition zone equal 18 and 16 mm respectively.

The [Zn (SSZ) $(H_2O)_4]$ $.3H_2O$ and [Cu_2 Ni $(SSZ)_2$ $(H_2O)_4Cl_4]$ $.6H_2O$ tested compounds exhibited potent antimicrobial effect especially for Gram-positive bacterial strains (*Staphylococcus aureas, Bacillus subtilis*) and fungal strain (*Candida albicans*) in comparison to the reference free ligand.

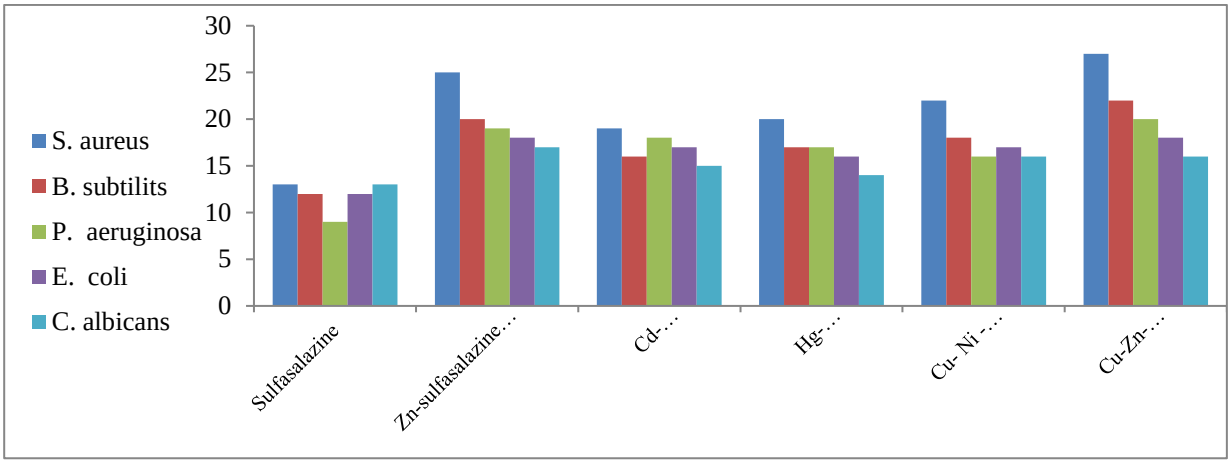

Figure 17: Biological assessment of sulfasalazine ligand and its metal complexes against 5 different species.

Table 7: Biological assessment for free sulfasalazine ligand and tested complexes against bacterial strains and Candida albicans.

Compound	**Inhibition zone diameter (mm/mg sample)**				
	Gram (+) Bacterial strain		**Gram (-) Bacterial strain**		**fungal strain**
	S. aureus	***B. subtilits***	***P. aeruginosa***	***E. coli***	***C. albicans***
Sulfasalazine	13	12	9	12	13
[Zn (SSZ) $(H_2O)_4$] $.3H_2O$	25	20	19	18	17
[Cd (SSZ) $(H_2O)_4$] $.2H_2O$	19	16	18	17	15
[Hg (SSZ) $(H_2O)_4$] $.3H_2O$	20	17	17	16	14
[Cu_2 Ni $(SSZ)_2$ $(H_2O)_4Cl_4$] $.6H_2O$	22	18	16	17	16
[$Cu_2Zn(SSZ)_2$ $(H_2O)_4Cl_4$] $.5H_2O$	27	22	20	18	16
Ciprofloxacin	30	30	30	30	-
Clotrimazole	-	-	-	-	18
DMSO	9	9	9	9	9

(b) The minimum inhibitory concentration (MIC): measure the lowest concentration required for microbial growth inhibition. MIC is helpful in research facilities because it may be used to track the activity of new antimicrobial medicines and monitor antibiotic resistance [52]. MIC is applied for some sulfasalazine-metal complexes that have highest antimicrobial activity results against tested species reported in Table (7), MIC results by µg/ml are summarized in Table (8).

Table 8: Minimum inhibitory concentration (MIC) by (µg/ml) of sulfasalazine metal complexes against bacterial strains and Candida albicans.

Compound	**Gram (+) Bacterial strain**		**Gram (-) Bacterial strain**		**fungal strain**
	S. aureus	***B. subtilits***	***P. aeruginosa***	***E. coli***	***C. albicans***
[Zn (SSZ) $(H_2O)_4$] $.3H_2O$	15.625	31.25	31.25	15.625	31.25
[Cu_2 Ni $(SSZ)_2$ $(H_2O)_4Cl_4$] $.6H_2O$	31.25	31.25	62.5	31.25	62.5
[$Cu_2Zn(SSZ)_2$ $(H_2O)_4Cl_4$] $.5H_2O$	15.625	31.25	31.25	15.625	31.25

The MIC of lowest concentration value is revealed from $[Cu_2Zn(SSZ)_2\ (H_2O)_4Cl_4]\ .5H_2O$ and $[Zn\ (SSZ)\ (H_2O)_4]\ .3H_2O$ complexes against (*S. aureus*, *E.Coli*) with the same value for both 15.625 µg/ml with higher antimicrobial activity. For (*B. subtilits*, *P. aeruginosa* and *C. albicans*) the previous two complexes showed MIC of 31.25 µg/ml.

3.8. Molecular docking

The in vitro assessment of any proposed biologically active chemical must be preceded by a docking investigation. This method clarifies the nature of interactions and the ligand-receptor location. Additionally, it provides an estimate of the distance inside the interaction grid between the ligand and the receptor. The degree of inhibitory effect of the associated ligand is reflected in the scoring energy of each position simulated by the docking computations [53].

Prostate cancer is one of the most common tumors in the world and the fifth leading cause of male cancer death. Although the treatment of localized androgen-dependent prostate cancer has been successful, the efficacy of androgen-independent metastatic disease is limited. This study aimed to use the 6XXO protein (prostate cancer protein) for the discovery of new targeted therapy [53-55].

To determine the most likely compound that can bind to the 6XXO protein, we docked the modeled 6XXO 3D structure against ligand (sulfasalazine) and some of its complexes ($[Zn\ (SSZ)\ (H_2O)_4]\ .3H_2O$, $[Cu_2\ Ni\ (SSZ)_2\ (H_2O)_4Cl_4]\ .6H_2O$ and $[Cu_2Zn(SSZ)_2\ (H_2O)_4Cl_4]\ .5H_2O$), drug candidates using Moldock score. Protein basic local alignment search tool (BLAST) search, multiple sequence alignment (MSA), and phylogenetics were further carried out to analyze the diversity of this marker and determine its conserved domains as suitable target regions.

The docked sulfasalazine with 6XXO which is responsible for prostate cancer, Figures (18,19), showed electrostatic and hydrogen bond between ligand and receptor interaction distances were ≤ 3.04 Å in most cases, which indicates the presence of typical real bonds which means high binding affinity. For example, the nearest interaction is observed *via* H-donors with 6XX0 (2.89 Å) and ligand. With Moldock score -7104.8 and scoring energy (S) -2.5 kcal, binding sites of designed drug with different amino acids (Ala 40, Glu 44 and Arg 38,) were observed which demonstrating their ability of inhibition of prostate cancer .

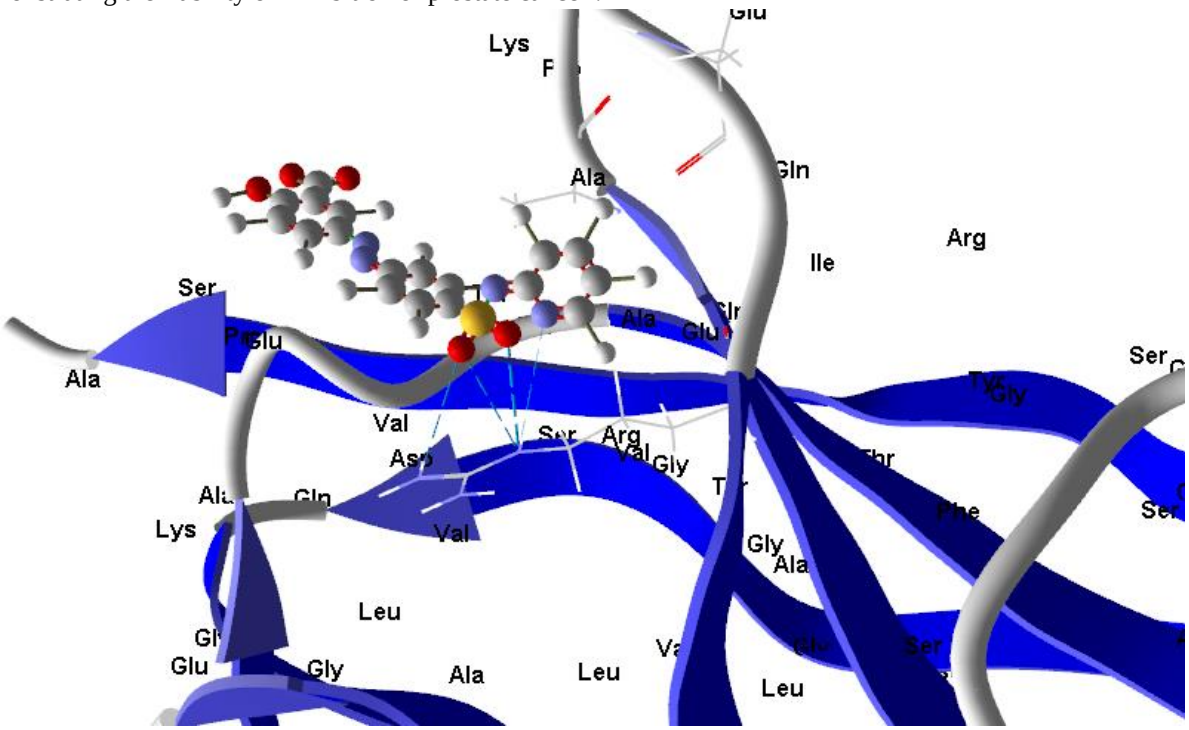

Figure 18: Virtual molecular docking of the best docked sulfasalazine with 6XXO protein

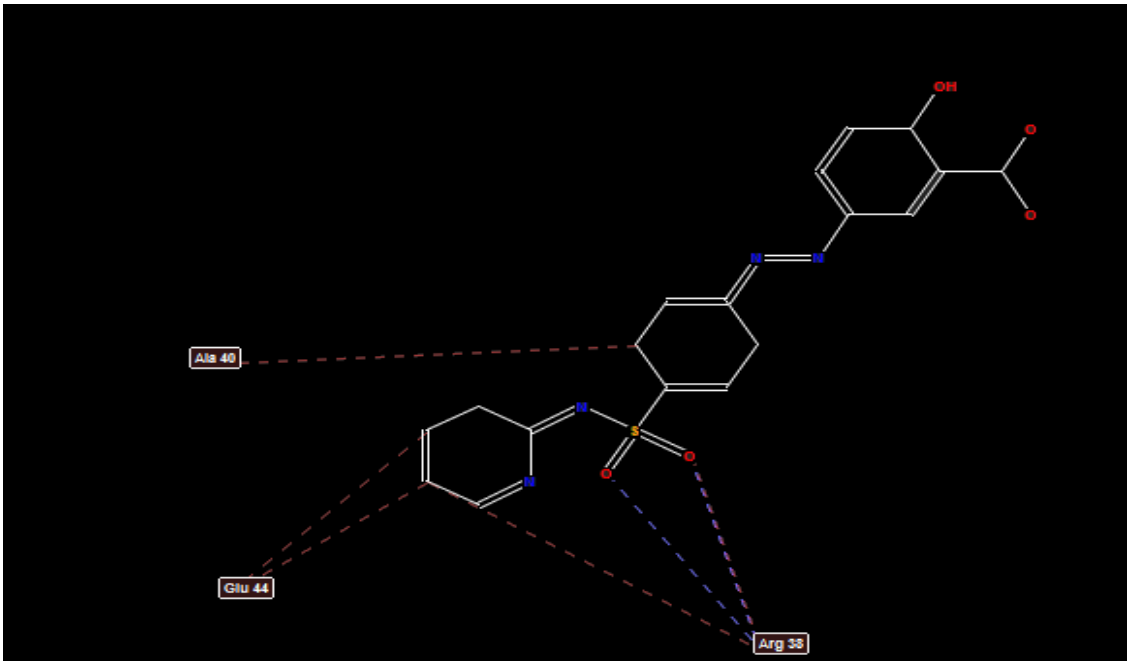

Figure 19: 2D structure of molecular docking of sulfasalazine with 6XXO protein

While the designed drug ([Zn (SSZ) $(H_2O)_4$] $.3H_2O$) is docked with 6XXO prostate cancer prostate, Figure (20,21), Showed an excellent electrostatic and hydrogen bond between ligand and receptor through one binding site .The nearest interaction is observed *via* H-donors with 6XX0 (3.11 Å) and (Zinc metal complex) which indicates the presence of typical real bonds With MolDock score -56206.8 , different binding sites of designed drug with different amino acids (Glu 89, Arg 38 and Ala 40) were observed which demonstrating their higher inhibition for 6XXO than ligand.

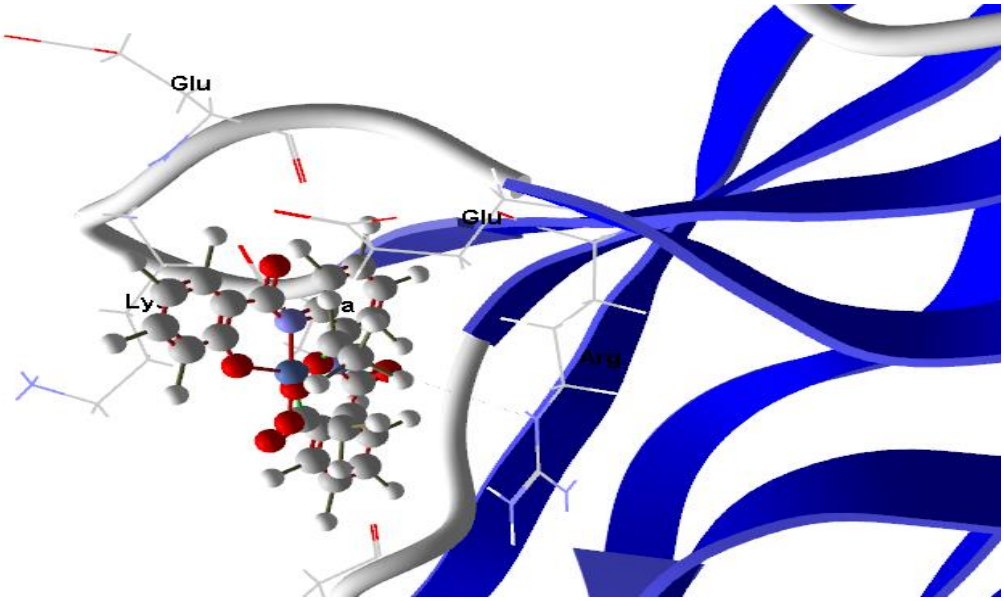

Figure 20: Virtual molecular docking of the best docked [Zn (SSZ) $(H_2O)_4$] $.3H_2O$ with 6XXO protein

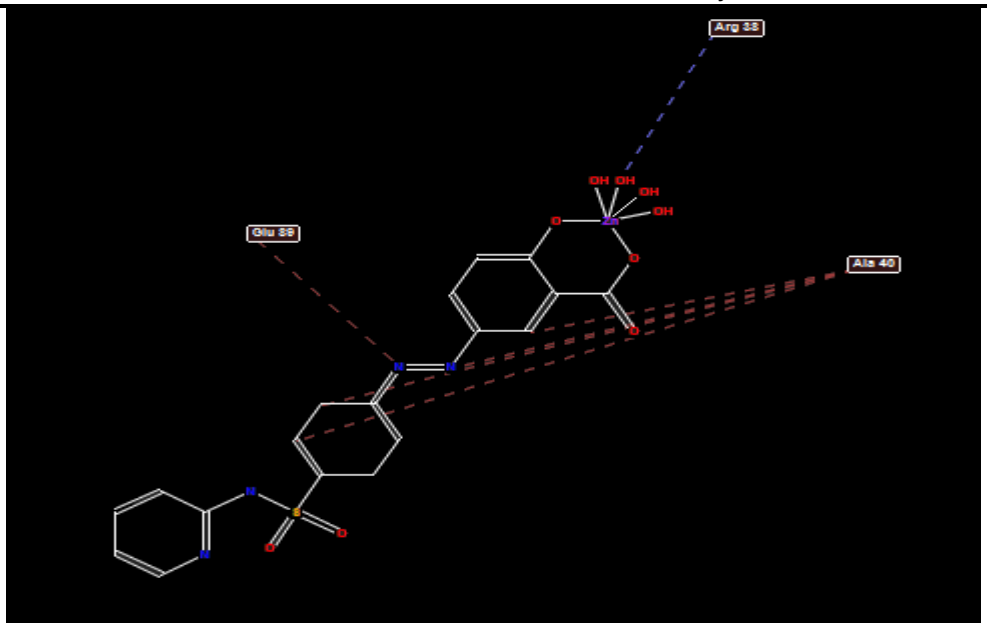

Figure 21: 2D structure of molecular docking of [Zn (SSZ) $(H_2O)_4$] .3H_2O with 6XX0 protein

However, ([Cu_2 Ni $(SSZ)_2$ $(H_2O)_4Cl_4$] .6H_2O) is docked with 6XXO prostate cancer prostate, Figure (22,23), showed an excellent electrostatic and hydrogen bond between ligand and receptor. The nearest interaction is observed *via* H-donors with 6XX0 (2.94 Å) and (Cu-Ni complex) which indicates the presence of typical real bonds which means high binding affinity With Moldock score (S) -167653 and plant score -126.984, the binding sites of designed drug with different amino acids (Ala 40, Ala 47, Glu 48, Glu 89, pro 41 and Arg 38) were observed which demonstrating their excellent inhibition representing the best one towards inhibition of prostate cancer protein.

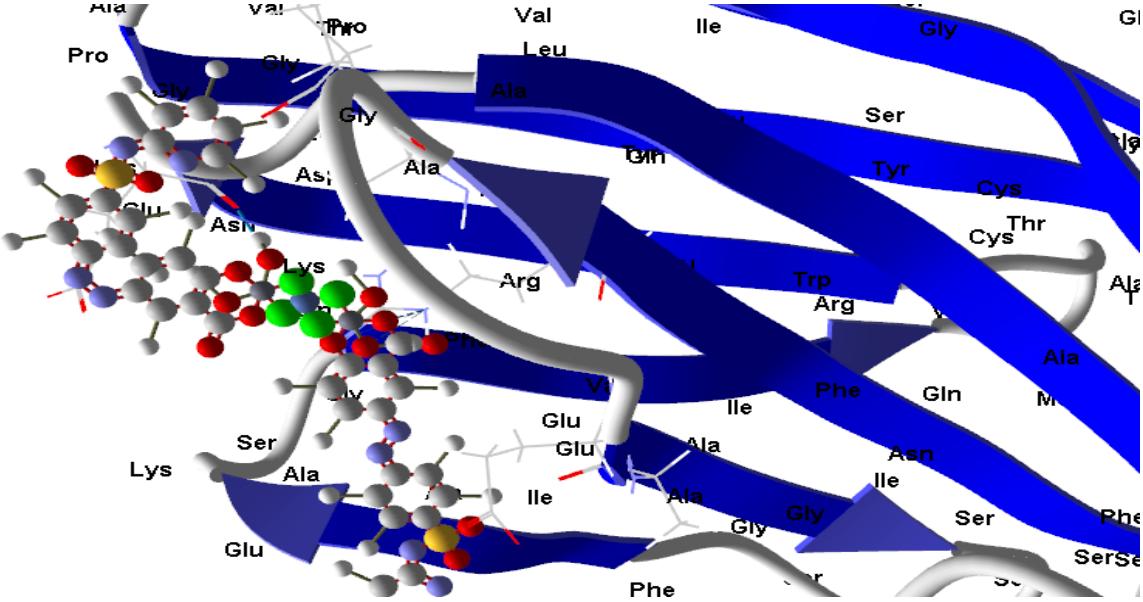

Figure 22: Virtual molecular docking of the best docked [Cu_2 Ni $(SSZ)_2$ $(H_2O)_4Cl_4$] .6H_2O with 6XXO protein

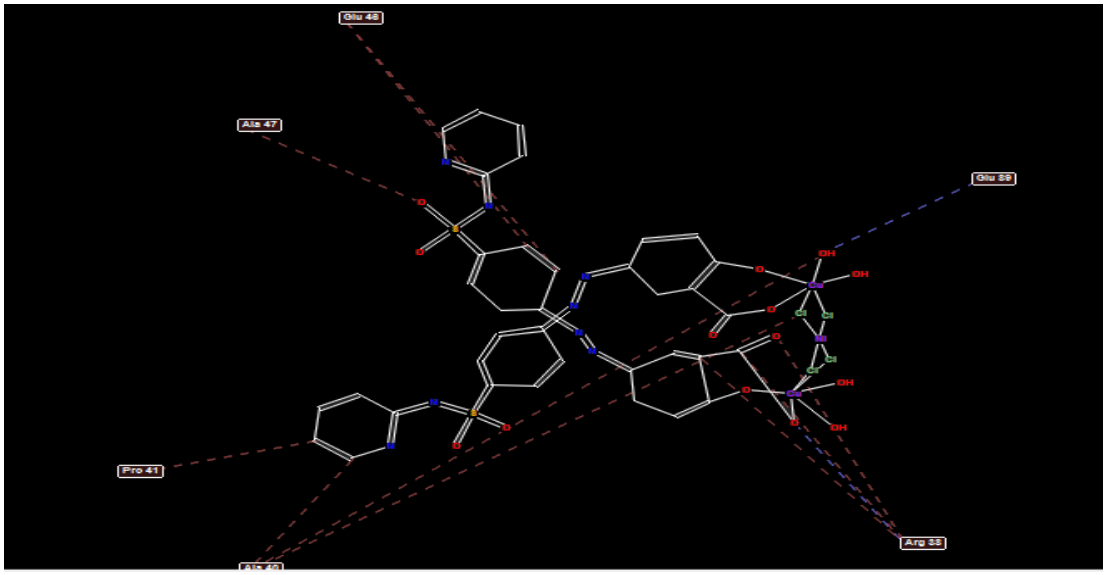

Figure 23: 2D structure of molecular docking of [Cu_2 Ni $(SSZ)_2$ $(H2O)_4Cl_4$] .6H_2O with 6XX0 protein.

While the docked [$Cu_2Zn(SSZ)_2$ $(H_2O)_4Cl_4$] .5H_2O with 6XXO prostate protein cancer , Figure (24,25), showed a good electrostatic and hydrogen bond between ligand and receptor interaction distances were ≤ 3.5 Å in most cases, which indicates the presence of typical real bonds which means high binding affinity . For example, the nearest interaction is observed via H-donors with 6XX0 (2.97 Å) and (Cu-Zn-complex) With MolDock score -124192 and plant score -1268, seven binding sites of designed drug with different amino acids (Ala 40,Ala 41, Ala 61, Glu 89,Thr 91, pro 41 and Arg 38) were observed represent the lowest one towards inhibition of prostate cancer protein.

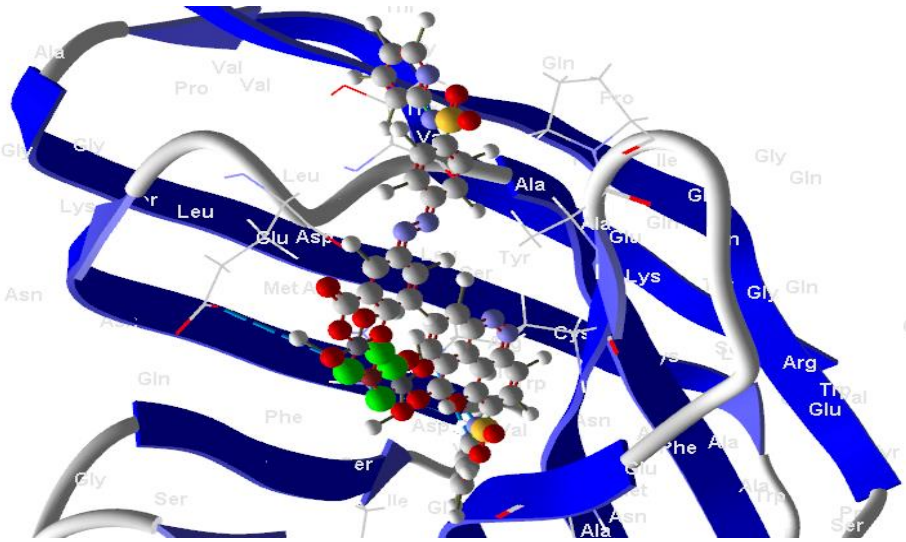

Figure 24: Virtual molecular docking of the best docked [$Cu_2Zn(SSZ)_2$ $(H_2O)_4Cl_4$].5H_2O with 6XXO protein.

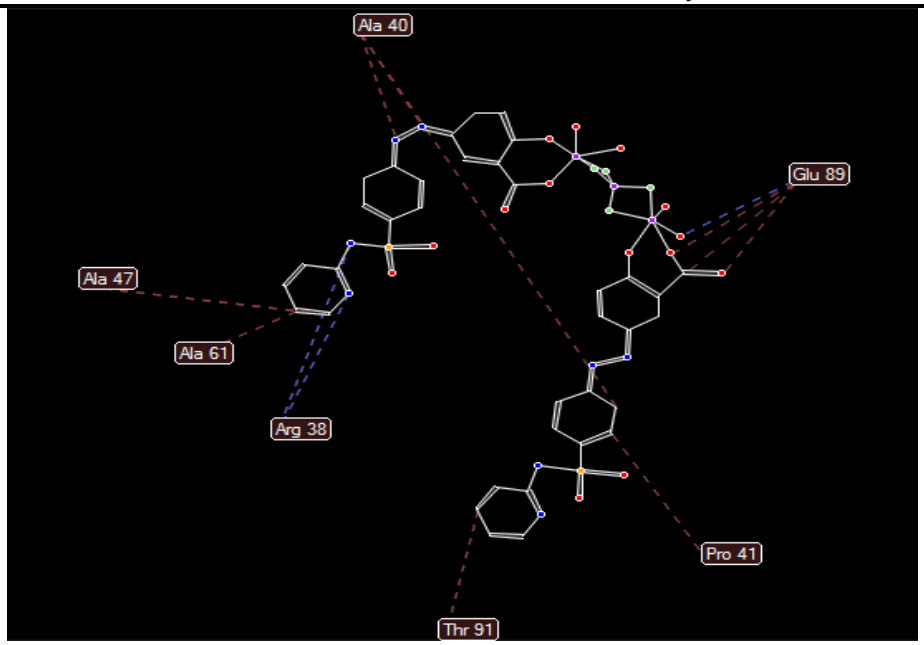

Figure 25: 2D structure of molecular docking of $[Cu_2Zn(SSZ)_2\ (H_2O)_4Cl_4]\ .5H_2O$ with 6XX0 protein

References

[1]. Sutherland, L., Roth, D., Beck, P., May, G., & Makiyama, K. (2000). Cochrane Database Syst. Rev. CD000543.

[2]. Volin, M. V., Campbell, P. L., Connors, M. A., Woodruff, D. C., & Koch, A. E. (2002). The effect of sulfasalazine on rheumatoid arthritic synovial tissue chemokine production. Experimental and molecular pathology, 73(2), 84-92.

[3]. Matasiæ, R., Dietz, A. B., & Vuk-Pavloviæ, S. (2001). Maturation of human dendritic cells as sulfasalazine target. Croat. Med. J, 42, 440-445.

[4]. Weisman, M. H. (2011). Rheumatoid arthritis. Oxford American Rheumatology L. Hanauer, S. B., Sandborn, W. J., Kornbluth, A., Katz, S., Safdi, M., Woogen, S., ... & Ajayi, F. (2005). Delayed-release oral mesalamine at 4.8 g/day (800 mg tablet) for the treatment of moderately active ulcerative colitis: the ASCEND II trial. Official journal of the American College of Gastroenterology| ACG, 100(11), 2478-2485.

[5]. Diav–Citrin, O., Park, Y. H., Veerasuntharam, G., Polachek, H., Bologa, M., Pastuszak, A., & Koren, G. (1998). The safety of mesalamine in human pregnancy: a prospective controlled cohort study. Gastroenterology, 114(1), 23-28.

[6]. Refat, M. S., & Mohamed, S. F. (2011). Spectroscopic, thermal and antitumor investigations of sulfasalazine drug in situ complexation with alkaline earth metal ions. Spectrochimica Acta Part A: Molecular and Biomolecular Spectroscopy, 82(1), 108^{-1}17.

[7]. O'Neil, M. J. (Ed.). (2013). The Merck index: an encyclopedia of chemicals, drugs, and biologicals. RSC Publishing.

[8]. Zheng, L., Duarte, M. E., Sevarolli Loftus, A., & Kim, S. W. (2021). Intestinal health of pigs upon weaning: challenges and nutritional intervention. Frontiers in Veterinary Science, 8, 628258.

[9]. Haynes, W. M. (Ed.). (2014). CRC handbook of chemistry and physics. CRC press.

[10]. Lewis, R. J., & Sax, N. J. N. Y. (1996). Sax's dangerous properties of industrial materials. New York, 3, 1928.

[11]. Das, R., Bej, S., Murmu, N. C., & Banerjee, P. (2022). Selective recognition of ammonia and aliphatic amines by CN fused phenazine derivative: A hydrogel based smartphone assisted 'opto-electronic nose'for

food spoilage evaluation with potent anti-counterfeiting activity and a potential prostate cancer biomarker sensor. Analytica Chimica Acta, 1202, 339597.

[12]. Liang, J., Xiong, H., Wang, W., Wen, W., Zhang, X., & Wang, S. (2018). "Luminescent-off/on" sensing mechanism of antibiotic-capped gold nanoclusters to phosphate-containing metabolites and its antibacterial characteristics. Sensors and Actuators B: Chemical, 255, 2170-2178.

[13]. Vardanyan, R., & Hruby, V. (2006). Synthesis of essential drugs. Elsevier.

[14]. Hu, G., Kang, J., Ng, L. W., Zhu, X., Howe, R. C., Jones, C. G., ... & Hasan, T. (2018). Functional inks and printing of two-dimensional materials. Chemical Society Reviews, 47(9), 3265-3300.

[15]. Nygård, B., Olofsson, J., & Sandberg, M. (1966). Some physico-chemical properties of salicylazosulphapyridine, including its solubility, protolytic constants and general spectrochemical and polarographic behaviour. Acta Pharmaceutica Suecica, 3(5), 313-342.

[16]. Matejovic, I. (1993). Determination of carbon, hydrogen, and nitrogen in soils by automated elemental analysis (dry combustion method). Communications in Soil Science and Plant Analysis, 24(17^{-1}8), 2213-2222.

[17]. Vogel, A. I. (1989). A textbook of quantitative inorganic analysis, theory and practice, ; revised by Jeffrey GH et al.

[18]. Lee, R. H., Griswold, E., & Kleinberg, J. (1964). Studies on the stepwise controlled decomposition of 2, 2'-bipyridine complexes of cobalt (II) and nickel (II) chlorides. Inorganic Chemistry, 3(9), 1278^{-1}283.

[19]. Kafarski, M., Szypłowska, A., Majcher, J., Wilczek, A., Lewandowski, A., Hlaváčová, Z., & Skierucha, W. (2022). Complex Dielectric Permittivity Spectra of Rapeseed in the 20 MHz–3 GHz Frequency Range. Materials, 15(14), 4844.

[20]. Reinen, D., & Friebel, C. (1984). Cu2+ in 5-coordination: a case of a second-order Jahn-Teller effect. II: CuCl53-and other CuIIL5 complexes: trigonal bipyramid or square pyramid?. Inorganic chemistry (Print), 23(7), 791-798.

[21]. Shebl, M. (2017). Coordination behavior of new bis (tridentate ONO, ONS and ONN) donor hydrazones towards some transition metal ions: Synthesis, spectral, thermal, antimicrobial and antitumor studies. Journal of Molecular Structure, 1128, 79-93.

[22]. Agwa, A., Aly, M. M., & Bonaly, R. (2000). Isolation and characterization of two Streptomyces species produced non polyenic antifungal agents. J. Union Arab Biol, 7, 62-84.

[23]. Baghban, R., Ghasemali, S., Farajnia, S., Hoseinpoor, R., Andarzi, S., Zakariazadeh, M., & Zarredar, H. (2021). Design and in silico evaluation of a novel cyclic disulfide-rich anti-VEGF peptide as a potential antiangiogenic drug. International Journal of Peptide Research and Therapeutics, 27, 2245-2256 .

[24]. Chen, G., Seukep, A. J., & Guo, M. (2020). Recent advances in molecular docking for the research and discovery of potential marine drugs. Marine drugs, 18(11), 545.

[25]. Masoud, M. S., Ali, A. E., & Elasala, G. S. (2015). Synthesis, spectral, computational and thermal analysis studies of metallocefotaxime antibiotics. Spectrochimica Acta Part A: Molecular and Biomolecular Spectroscopy, 149, 363-377.

[26]. (a) Brammer, L., Burgard, M. D., Eddleston, M. D., Rodger, C. S., Rath, N. P., & Adams, H. (2002). Designing neutral coordination networks with the aid of hydrogen bond mimicry using silver (i) carboxylates. CrystEngComm, 4, 239-248.

(b)- Libri, S., Mahler, M., Mínguez Espallargas, G., Singh, D. C., Soleimannejad, J., Adams, H., ... & Brammer, L. (2008). Ligand Substitution within Nonporous Crystals of a Coordination Polymer: Elimination from and Insertion into Ag□ O Bonds by Alcohol Molecules in a Solid–Vapor Reaction. Angewandte Chemie International Edition, 47(9), 1693^{-1}697.

[27]. Li, C. P., Chen, J., Yu, Q., & Du, M. (2010). Structural modulation and properties of silver (I) coordination frameworks with benzenedicarboxyl tectons and $trans^{-1}$-(2-pyridyl)-2-(4-pyridyl) ethylene spacer. Crystal growth & design, 10(4), 1623^{-1}632.

[28]. Ali AE, Elasala GS, Ibrahim RS and Kolkaila AS (2021). Synthesis, characterization, spectral, thermal analysis and biological activity studies of some montelukast sodium complexes. Journal of Chemical Research Advances, 02(01): 26-41.

[29]. Soliman, A. A., Mohamed, G. G., Hosny, W. M., & El-Mawgood, M. A. (2005). Synthesis, spectroscopic and thermal characterization of new sulfasalazine metal complexes. Synthesis and Reactivity in Inorganic, Metal-Organic, and Nano-Metal Chemistry, 35(6), 483-490.

[30]. Santi, E., Torre, M. H., Kremer, E., Etcheverry, S. B., & Baran, E. J. (1993). Vibrational spectra of the copper (II) and nickel (II) complexes of piroxicam. Vibrational spectroscopy, 5(3), 285-293.

[31]. Mohamed, G. G. (2001). Metal complexes of antibiotic drugs. Studies on dicluxacillin complexes of FeII, FeIII, CoII, NiII and CuII. Spectrochimica Acta Part A: Molecular and Biomolecular Spectroscopy, 57(8), 1643^{-1}648.

[32]. Masoud, M. S., Ali, A. E., & Elasala, G. S. (2015). Synthesis, spectral, computational and thermal analysis studies of metalloceftriaxone antibiotic. Journal of Molecular Structure, 1084, 259-273.

[33]. Masoud, M. S., El-Marghany, A., Orabi, A., Ali, A. E., & Sayed, R. (2013). Spectral, coordination and thermal properties of 5-arylidene thiobarbituric acids. Spectrochimica Acta Part A: Molecular and Biomolecular Spectroscopy, 107, 179^{-1}87.

[34]. Masoud, M. S., Ali, A. E., Ghareeb, D. A., & Nasr, N. M. (2015). Structural, spectral and thermal analysis of some metallocephradines. Journal of Molecular Structure, 1099, 359-372.

[35]. Masoud, M. S., Ali, A. E., Elasala, G. S., & Elwardany, R. E. (2019). Structural and thermal studies on some morpholine complexes. Journal of Molecular Structure, 1175, 648-662.

[36]. Masoud, M. S., Soayed, A. A., & El-Husseiny, A. F. (2012). Coordination modes, spectral, thermal and biological evaluation of hetero-metal copper containing 2-thiouracil complexes. Spectrochimica Acta Part A: Molecular and Biomolecular Spectroscopy, 99, 365-372.

[37]. Bolton, J. R., & Wertz, J. E. (1972). Electron spin resonance: elementary theory and practical applications. McGraw-Hill. New York, Library of Congress Catalog Number 77^{-1}54239, PP.449.

[38]. Sawant, V. A., Yamgar, B. A., Sawant, S. K., & Chavan, S. S. (2009). Synthesis, structural characterization, thermal and electrochemical studies of mixed ligand Cu (II) complexes containing 2-phenyl-3-(benzylamino)$^{-1}$, 2-dihydroquinazoline-4-(3H)-one and bidentate N-donor ligands. Spectrochimica Acta Part A: Molecular and Biomolecular Spectroscopy, 74(5), 1100^{-1}106.

[39]. Choi, J., Park, M. H., Shin, S. H., Byeon, J. J., Lee, B. I., Park, Y., & Shin, Y. G. (2021). Quantification and metabolite identification of sulfasalazine in mouse brain and plasma using quadrupole-time-of-flight mass spectrometry. Molecules, 26(4), 1179.

[40]. Noriega, P., Gortaire, G., & Osorio, E. (2021). Mass Spectrometry and Its Importance for the Analysis and Discovery of Active Molecules in Natural Products. Natural Drugs from Plants. (book)

[41]. Mohamed, E. A., Ali, A. E., Kolkaila, S. A., Fyala, S. S., & Elasala, G. S. Synthesis, Spectroscopic Studies, Thermal Analysis and Molecular Docking of Chloramphenicol Metal Complexes as Anti-Prostate Cancer. TWIST, 2024,19(1), 400-408.

[42]. Kolkaila S.A., Ali A.E., Mustafa Ahmed A. Removal of Aluminum (III) from Water by Adsorption on the Surface of Natural Compound. J. of Environmental Treatment Techniques,2023 11(2) 10^{-1}05.

[43]. Ali A.E., Elasala G.S., Rana M. Atta. and kolkaila S.A., Synthesis, Thermal Analysis and Characterization of Doxycycline Metal Complexes, Chemistry research journal. 2023, 7,2,90-91

[44]. Ali A. E., Elasala G. S., Eldeeb M. H., kolkaila S. A. Synthesis and Biological Activity and Thermal Analysis of Sulfaquinoxaline Mixed Metal Complexes. Journal of Chemistry & its Applications. 2023, SRC/JCIA^{-1}19.DOI: doi.org/10.47363/JCIA/2023(2)119

[45]. El-Tabl, A. S., El-Wahed, M. M. A., El Kadi, N. M., Kolkaila, S. A., & Samy, M. Novel Metal Complexes of Bioactive Amide Ligands as New Potential Antibreast Cancer Agents. TWIST, 2023,18(4), 151-169.

[46]. El-Tabl, A. S., Kolkaila, S. A., Abdullah, S. M., & Ashour, A. M. Nano-Organometallic Compounds as Prospective Metal BasedAnti-Lung Cancer Drugs: Biochemical and Molecular Docking Studies. TWIST, 2023,18(4), 141-150.

[47]. El-Tabl, A. S., Dawood, A. A. E. R., Kolkaila, S.A., Mohamed, E. H., & Ashour, A. The Cytotoxicity of Some Biologically Active Nano Compounds against Colon Cancer: 67- Advanced Biochemical Analyses. TWIST, 2023,18(4), 360-371.

[48]. El-Tabl, A. S., Abd El-Wahed, M. M., Kolkaila, S. A., Abd El-Nasser, A. G., & Ashour, A. M. Biochemical Studies on Some Novel Organometallic Complexes as Anti-Human Prostate Cancer. TWIST, 2024,19(1), 16-26.

[49]. Kolkaila S.A., Ali A.E. and Elasala G.S., Synthesis, Spectral Characterization of Azithromycin with Transition Metals and a Molecular Approach for Azithromycin with Zinc for COVID-19. 2021, Int J Cur Res Rev.13, 23, 53-59.

[50]. Masoud M.S., Ali A.E., Elasala G.S. and Kolkaila S.A., Synthesis, spectroscopic, biological activity and hermal characterization of ceftazidime with transition metals. Spectrochim. Acta. 2018,193, 458-466.

[51]. Ali A. E., Elasala G. S., Mohamed E. A. and Kolkaila S.A., Spectral, thermal studies and biological activity of pyrazinamide complexes heliyon, 2019, 5(11).

[52]. Ali A.E., Elasala G.S., Mohamed E. A. and Kolkaila S.A., Structural and thermal analysis of some imipramine complexes. J. materials today proceeding. 2021.

[53]. Masoud M.S., Ali A.E., Elasala G.S. and Kolkaila S.A., Synthesis, Spectroscopic Studies and Thermal Analysis on Cefoperazone Metal Complexes. J. Chem. Pharm. Res. 2017, 9(4), 171-179.

[54]. Elasala, G. S., Fyala, S. S., & Ali, A. E. (2023). Spectroscopic Studies, Thermal Analysis and Molecular Docking of Amikacin Metal Complexes. Chemistry Research Journal, 8(2),32-41.